Green Synthesis of ZnO Coated Porous Activated Carbon Prepared from Pontederia crassipe Leaves for the Adsorptive Removal of Toxic Organic Dyes

Mahmood A. Albo Hay Allah
Ministry of Education, Educational Directorate of Karbala
Hassan A. Alshamsi (hassan.habeeb@qu.edu.iq)
University of Al-Qadisiyah

Research Article

Keywords: Green synthesis, Pontederia crassipes, ZnO NPs, Activated carbon, Adsorption, Congo red, Malachite Green, Wastewater treatment

Posted Date: January 27th, 2023

DOI: https://doi.org/10.21203/rs.3.rs-2508076/v1

Additional Declarations: No competing interests reported.

Green Synthesis of ZnO Coated Porous Activated Carbon Prepared from *Pontederia crassipe* Leaves for the Adsorptive Removal of Toxic Organic Dyes

Mahmood A. Albo Hay Allah[1, 2], Hassan A. Alshamsi[3*]

[1]Ministry of Education, Educational Directorate of Karbala, Iraq

[2]University of Warith Al-Anbiyaa, College of Nursing, Karbala, Iraq

[3]University of Al-Qadisiyah, College of Education, Department of Chemistry, Republic of Iraq

Corresponding author E-mail: hassan.habeeb@qu.edu.iq

Abstract

In the current study, new zinc oxide/activated carbon (ZnO/AC) nanocomposites were successfully synthesized, using *Pontederia crassipes* leaves as a carbon source for synthesis of activated carbon. In addition, the extract of *Pontederia crassipes* leaves was obtained as reducing and capping agent in the synthesis of ZnO. The synthesized materials were investigated using various characterization techniques including XRD, FTIR, FE-SEM, EDX, BET-BJH, TEM and Raman, which proved the successful synthesis. The synthesized samples were applied as new nanoadsorbents for the uptake of Malachite Green (MG) and Congo Red (CR) dyes from aquatic media. The thermodynamic, adsorption isotherm and kinetic studies were conducted adopting the batch experiment method. The results showed that the optimum efficiency of removal of both dyes was achieved with ZnO/AC (10%) nanocomposite, which was found to be 98.87% for CR dye and 99.23% for MG dye. The thermodynamic analysis exhibited that adsorption process for both dyes is spontaneous. In addition, the results exhibited that the removal of CR onto ZnO/AC(10%) was exothermic, while that of MG was an endothermic. In the case of adsorption isotherms, the Freundlich model showed the best fit for both dyes with a high correlation coefficient (R^2) of 0.99, suggesting heterogeneous surface of the synthesized nanoparticles. The kinetic analysis indicated that both dyes followed a pseudo-second-order kinetic model.

Keywords: Green synthesis. *Pontederia crassipes*. ZnO NPs. Activated carbon. Adsorption. Congo red. Malachite Green. Wastewater treatment.

Introduction

Nowadays, water scarcity, water pollution and water quality are among the most important environmental issues. Technological progress has brought the world new issues along with contamination problems and environmental disorders. Aquatic pollution mainly results from the discharge of domestic, industrial, and municipal wastes including the colored effluents, which are considered as one of the biggest pollutants. In many cases, water pollution is due to contamination by inorganic and/or organic compounds including colored substances. In particular, the presence of

colored materials in water, or in general, in effluents should be avoided because they are toxic, mutagenic, and carcinogenic, towards organisms' life and humans (Lellis et al. 2019). Synthetic dyes are widely used in industries such as textiles, printing, rubber, paper, plastics, pharmaceuticals, leather, cosmetics, etc. (Slama et al. 2021). Most of organic dyes possess complex and highly branched aromatic molecular structures (Thomas et al. 2019). Textile effluents are intensively colored due to unfixed organic dyes on fibers and these materials must be isolated or treated before being discharged into the surrounding environment where approximately 30% of the world's dye production might be wasted during the dying process (Suresh et al. 2014). Thermal wastewater treatment, which is based on aerobic biodegradation, has a low removal efficiency of most organic dyes (Sheng et al. 2018). Direct discharge of colored wastewater into the environment can be hazardous due to the most of dyestuff are highly resistant to the biodegradation treatment process, hence it is usually processed either by a physical or chemical processes (Daud et al. 2022). Congo red (CR) and malachite green (MG) dyes are two examples of frequently organic compounds that are used in textile industry. The presence of MG in aquatic media has negative consequences on aquatic environment and human health. MG damages the spleen, lever, heart and kidneys (Srivastava et al. 2004). Accordingly, CR dye is spread in various industries, including rubber, plastic, paper, and textile (Aminu et al. 2020). In water, Congo red transforms into a red colloidal solution, expecting metabolize to stable aromatic compound, benzidine, a substance that has been classified to be mutagenic to aquatic organisms and carcinogenic to human (Swan et al. 2019).

Various physical, chemical and biological treatment techniques methods such as coagulation, reverse osmosis, ionization exchange, photocatalysis, oxidation, adsorption and ozone treatments are used to remove dyes from water and wastewater (Mokif et al. 2019; Vijayageetha et al. 2014; Huang et al. 2021; Torkian et al. 2022; Chanikya et al. 2021; Alwan et al. 2022; Powar et al. 2020; Ajel et al. 2022). Most of these techniques are characterized by high efficiency in treating colored water, but their major disadvantage is the high operating cost. Among the efficient methods, adsorption technology is widely used in removing organic and inorganic pollutants from water and wastewater. Adsorption can be considered as an effective wastewater treatment process due to its low cost, ease of operation and high efficiency. Materials that can be used as dye absorbents include activated carbon, zeolite, clay, agricultural solid waste, chitosan, metal oxides, polymers, carbon nanotubes, and graphene (Sheeja et al. 2021; Hammood et al. 2021; Martinez et al. 2019; El-Bery et al.2022; Ibrahim et al. 2020; Elfeky et al. 2020; Mok et al. 2020; Kar et al. 2020; Poton et al. 2022). Activated carbon is one of the most efficient and low cost materials to remove colored materials from polluted water, perhaps due to the high surface area associated with its porous structure (Kheddo et al. 2020). Specific surface area and surface activation are usually required to obtain better catalytic and surface properties. The efficiency

of adsorption may be affected by the composition of the raw materials and the carbonization temperature (Maniarasu et al. 2022). The main feature of obtaining activated carbon to provide efficient adsorptive removal of a wide variety of organic materials, to be environmentally friendly material. Activated carbon derived from biomass resources has proven to be a versatile material due to its ability to remove various water pollutants related to its high active adsorption sites (Hamad et al. 2022). In addition to hydrothermal carbonization, the most reliable technology for producing activated carbon is the chemical activation of carbon sources followed by carbonization at an inert atmosphere and high temperatures (Ma et al. 2017). The most important chemically activated agents are sulfuric acid (H_2SO_4), phosphoric acid (H_3PO_4), hydrochloric acid (HCl), nitric acid (HNO_3), potassium hydroxide (KOH), sodium hydroxide (NaOH), zinc chloride ($ZnCl_2$) , ferric chloride ($FeCl_3$), calcium carbonate ($CaCO_3$), and potassium carbonate K_2CO_3 (Chen et al. 2017; Khalili et al. 2016; Purnaningtyas et al. 2020).

Recently, due to their exceptional physical and chemical properties, zinc oxide nanoparticles (ZnO NPs) have attracted great attention among other nanoparticles due to their unique properties such as non-toxicity, low cost, and high photocatalytic and photochemical activities (Ameen et al. 2021). ZnO NPs and their nanocomposites were explored to adsorb various industrial dyes in addition to other water pollutants, and previous studies showed that zinc oxide is an effective adsorbent for removing many pollutants (Bharti et al. 2022; Zafar et al. 2019). ZnO is biocompatible and facile in synthesis, while environmental situations do not alter its structural properties (Mohd et al. 2019). Several methods have been used to synthesis zinc oxide such as soft chemical method, sol-gel process, vapor phase growth, vapor-liquid-solid process, electrophoretic deposition, thermal evaporation, homogeneous deposition, chemical vapor deposition and chemical bath deposition (Nasrollahzadeh et al. 2018; Bhuiyan et al. 2021). In most chemical synthetic processes, hazardous chemical as reducing agents have been obtained as a stabilizing agent to controlling particle growth and suppress aggregations/agglomerations. The interest in the manufacturing of ecofriendly nanoparticles has been expanded significantly in the recent years. Biological synthesis approaches have been adduced as efficient ecofriendly processes for nanomaterials synthesis. Biological approaches, however, utilize low cost, eco-friendly biomolecules from plants, agricultural waste, fungi, and bacteria instead of harsh chemicals and expensive conventional methods. The use of various natural sources, particularly plant parts and plant extracts for fabrication of nanomaterials has many advantages over chemical synthesis methods such as cost effectiveness, simplicity, ecofriendliness, safety, biocompatibility, and high scale productivity (Jan et al. 2021). Plant extracts supply safe phytochemicals that are naturally abundant, environmentally friendly, biocompatible, and cheap. Thus, these safe biomolecules are the effective alternative to harmful chemicals. The phytochemicals found in the plant extracts play an important

role as reducing, stabilizing, and capping agents, which in result influence the characteristics of synthesized nanoparticles.

Different plant extracts and their products have been adopted as alternative materials to synthesis nanomaterials via environmentally friendly approaches. To enhance the adaptive capacity for effective adsorption, activated carbon can be included with metal oxides such as ZnO. Synthesis of activated carbon-based nanocomposites can improves excellent characteristics such as enhanced surface porosity that is reflected in a high adsorption efficiency. The ZnO/AC nanocomposites can be adopted as effective systems for environmental treatment due to the synergistic impact arising from AC and ZnO particles that can enhance the removal efficacy .These nanocomposites have high reusability and can be used several times without losing their efficacy. In several studies, zinc oxide nanoparticles were combined with activated carbon to obtain porous carbon nanoparticles containing zinc oxide with effective adsorption performance (Nie et al. 2022; Yan et al. 2021). The synergistic roles of both ZnO and AC can arise from the efficient porosity and enhanced surface, which can induce efficient adsorption and removal processes of various organic and inorganic pollutants (Alhan et al. 2019). By incorporating zinc oxide with activated carbon, pores will be created and the pore size distribution will be better regulated (Nie et al. 2022). The current study is reflected in the use of the *Pontederia crassipe* leaves as an inexpensive and renewable source in the preparation of AC/ZnO nanocomposites. The dried leaves was obtained as a carbonaceous source for AC synthesis, while the fresh plant leaves extract was adopted as s both reducing and stabilizing agent for synthesized ZnO NPs. To our knowledge, there has not yet been a report on AC/ZnO nanocomposites fabricated using *Pontederia crassipe* leaves. Thus, it is very important to study environmentally friendly AC/ZnO synthesis technology to explore its characteristics and to efficiently utilize natural resources. *Pontederia crassipe* is a free-floating aquatic and overgrown plant in many countries and it adapted to live in different environments. *Pontederia crassipe* is a widely available plant for use in medicinal field. As previously reported, aqueous *Pontederia crassipe* leaf extract contain various biomolecules such as, phenolic compounds, alkaloids, flavonoids, sterls, and saponins, which may have considerable reducing/stabilizing features, exhibiting it as a promising candidate for ZnO NPs synthesis (Pottail et al. 2012). In addition, the obtaining *Pontederia crassipe* leaves for AC synthesis may has significant importance. Also, this study aims to investigate the adsorptive removal of cationic dye, Congo red and anionic dye, Malachite green from aquatic media.

Materials and methods

Chemicals

Zinc nitrate hexahydrate ($Zn(NO_3)_2$.$6H_2O$, 99%), Malachite green dye ($C_{52}H_{54}N_4O_{12}$, M.Wt. = 927 g/mol), potassium chloride (KCl, 99%), Congo red dye ($C_{32}H_{22}N_6Na_2O_6S_2$ M.wt.= 696.7 g/mol)], , and Phosphoric acid (H_3PO_4, 85%) were purchased from Merck. Hydrochloric acid (HCl, 37%), Sodium chloride (NaCl, 99%), Sodium hydroxide (NaOH, 99%), and calcium chloride ($CaCl_2$, 99%) were supplied by Scharlau.

Preparation of *Pontederia crassipes* leaf extract

The extract of *Pontederia crassipes* leaves was prepared by procedure reported recently with slight modifications (Albo Hay Allah et al. 2022). Fresh wet leaves of *Pontederia crassipes* leaves were picked from water channels around Al-Diwaniyah city (southern Iraq). The collected leaves were thoroughly washed several times using tap water then distilled water to eradicate dust and other adhering materials. Afterwards, the leaves have been cut into small pieces. Briefly, 10 g of chopped leaves was immersed into 100 ml of distilled water at an adjusted temperature of 70°C for 30 min where the solution is constantly stirred using magnetic stirrer at a speed of 150 rpm. Finally, the suspended components were removed by filtration, and the supernatant was stored in a refrigerator at 4°C until to be utilized in the ZnO synthesis.

Synthesis of ZnO NPs

In the current work, modified method of previous report on green synthesis of ZnO NPs have been followed (Jayachandran et al. 2021). Briefly, 1.485 g of $Zn(NO_3)_2$. $6H_2O$ was added to 90 mL DDW followed by addition of 10 mL of leaves extract. Then, the solution was subjected to continuous stirring for 2 h using magnetic stirrer. This was followed by slow addition of sodium hydroxide (1 M) until the solution pH reached 10 while stirring continued for an additional 6 h at 70°C. This led to the accumulation of green-reduced product at the bottom of the vessel that observed as a yellowish white precipitate. The formed precipitate was collected using centrifugation at 8000 rpm for 20 min. Finally, the resultant product was subjected to repeated washing with distilled water by centrifugation 20 minute and dried by a vacuum oven at 80°C for 4 h.

Preparation of activated carbon

Fresh *Pontiteria crassipes* leaves have been obtained as a carbon source for synthesis of activated carbon. The collected leaves were completely rinsed several times using DW to remove the adherent impurities, then the clean leaves were chopped small pieces, then it was dried under sunlight for 6 days, followed by rinsing with ethanol and oven drying at 105°C overnight. Afterwards, the dried product was finely ground to a fine powder of 100 µm. After that, 10 g of sieved powder was added into 40 ml of 85% phosphoric acid solution in a ratio of 1:4 followed by stirring at 150 rpm for 30 min, then leave the solution to soak for 24 hours in the room temperature. When the activation was finished,

the solution was centrifuged and the resultant product was dried at 105°C for 24 h. Then, the dried sample was carbonized at 600°C for 4 h under N_2 atmosphere (Xu et al. 2014). The pyrolysis process of *Pontiteria crassipes* dry leaves yielded 24.7% of carbon**.**

Preparation of ZnO/activated carbon

The ZnO/AC nanocomposites were fabricated by dissolving 1.4875 g of $Zn(NO_3)_2 6H_2O$ into 90 mL of DW and 10 mL of aqueous extract of *Pontiteria crassipes* leaves was added. Then, the solution was steadily agitated on a magnetic stirrer for 2 h followed by a gradual addition of NaOH solution (1M) until the pH reached value of 10. Afterwards, an appropriate amount of activated carbon prepared in a previous step was suspended into the above solution, while the stirring was continuing for an additional 6 hours at 70°C. The resulting gray produce was centrifuged at 8000 rpm for 30 min followed by drying in a vacuum oven at 70°C for 4 h. Finally, the powder was kept in an airtight glass container for further use. The synthesis process of ZnO/AC samples is schematically illustrated in the Fig 1**.**

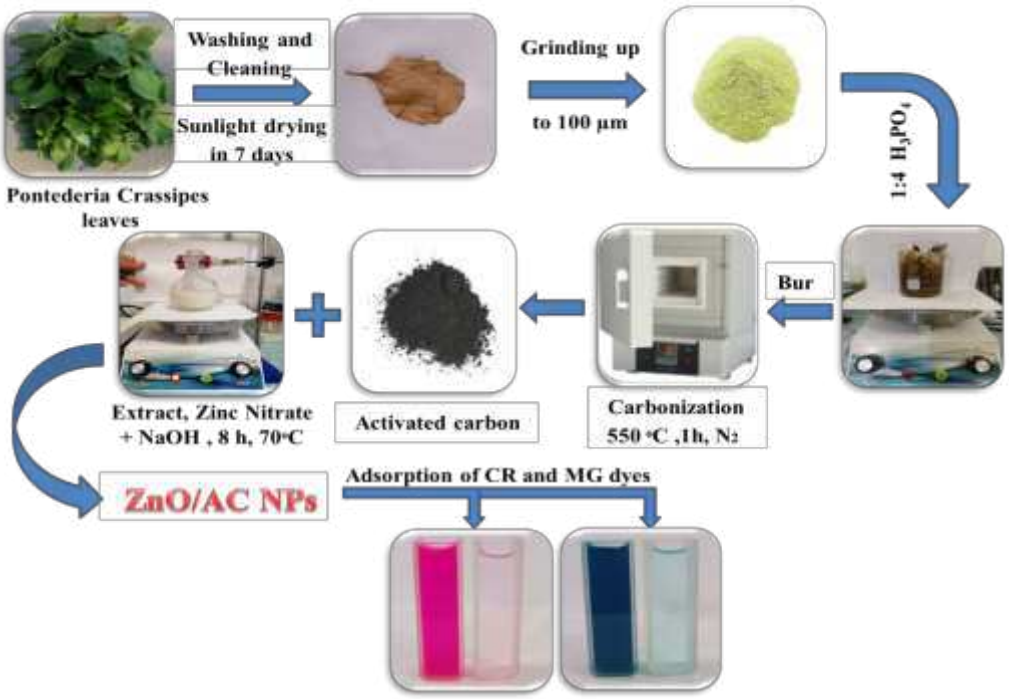

Fig. 1. Schematic diagram for the synthesis of ZnO/AC NPs

Characterization and instrumentations

Various characterization techniques were employed to investigation of physicochemical characteristics of synthesized materials. The XRD patterns were recorded with a PANalytical X'Pert Pro powder diffractometer, using CuK radiation ($\lambda = 0.154056$ nm) and a scanning range of 0° to 80°. To identification of functional groups in as synthesized nanomaterials, FT-IR spectra were collected with the wavenumber range of 500–4000 cm^{-1} by using Nicolet 6700 FT-IR spectrometer adopting KBr disks method. Scanning electron microscopy (ZEISS SIGMA VP) was used to study the surface

morphological features and particle size distribution as fabricated samples. Elemental composition of synthesized samples was determined during FE-SEM analysis using an Oxford EDS device. Transmittance electron microscopy (ZEISS-EM10C-100 KV) was employed to investigate the shape and particle sizes as-fabricated NPs. Raman spectra were analyzed by a micro Raman spectrometer (Takram, 785 nm Laser). Surface texture of synthesized materials was estimated using Quantachrome Instruments (Nova 2200e, USA). In addition, UV-Vis spectrophotometer (UV-1650, Shimadzu, Japan) was used to measure the absorption spectra of dye solutions.

Batch adsorption experiment

Batch adsorption method was conducted to study the sorption behavior of synthesized nanomaterials. In this regard, the impact of equilibrium time (0-120 min), adsorbent amount (0.01-0.2 g/L), solution pH (2-10), initial CR concentration (50- 500 mg/L) and initial MG concentration (75-250 mg/L), solution temperature (288-318K), and ionic strength (0.02-0.21) on the adsorption of CR and MG was investigated. For each batch process, in 150 mL conical flask, specific amount of adsorbent was suspended into 100 mL of dye solution. The solution pH was regulated using 0.1 M HCl or 0.1 M NaOH. The flask was agitated at 150 rpm, using incubated orbital shaker at constant temperature. After specified time intervals, the suspension was centrifuged at 8000 rpm for 15 min and the absorbance of supernatant was recorded at λ_{max} of dye (617 nm for MG and 495 nm for CR). Accordingly, the above steps were followed by changing one of the parameters while fixation others. At each time interval, the adsorption efficiency (%) and adsorption capacity (Q_e) were estimated using eqns. (1) and (2), respectively (Hassain et al. 2020):

$$Removal\ \% = \frac{C_o - C_e}{C_o} * 100 \quad (1)$$

$$Q_e = V(C_o - C_e)/\ m \quad (2)$$

Where C_o and C_e represent the initial concentration and the residual dye concentration in solution at time t (mg/L), V is the volume of dye solution (L), and m (g) is the s the mass of the adsorbent used.

Results and Discussion

Synthesis of ZnO and AC

Synthesis of ZnO NPs was firstly confirmed by visual observation of yellowish white product formation. Similar color changes of synthesized ZnO NPs using *Pelargonium odoratissimum* (L.) aqueous leaf extract were reported confirming the successful biosynthesis of ZnO NPs (Abdelbaky et al. 2022). As previously reported, the leaves of *Pontederia crassipe* plant are rich with various diverse bioactive secondary metabolites like alkaloids, flavonoids, phenolics, fatty acids, sterols, tannins, saponins, amino acids and other compounds (Ben Bakrim et al. 2022). Due to containing these phytochemicals various functional groups such as amines, hydroxyl and carboxyl, so they can contribute as reducing, stabilizing and capping agents in the synthesis of ZnO NPs. In general, when

the phytochemicals of *Pontederia crassipe* leaf extract contact with Zn^{2+} ions, the reducing agents donate their electrons to the Zn^{2+} and convert it stable nanoparticles (Alamdari et al. 2020). After the Zn^{2+} ions are completely reduced Zn metal, a reaction take place between zinc partiles and dissolved oxygen in the solution, resulting in the formation of ZnO nanoparticles (Yassin et al. 2022). *Pontederia crassipe* biomass (both leaf and stem) contain high water content (92.8-95%), and the remainder represent volatiles, protein and fibrous cellulose (Asep et al. 2017). The dry matter of *Pontederia crassipe* (~5-7.2% as weight ratio) is composed of cellulose (18.2 to 19%), hemicellulose (48.7 to 50%), lignin (3.5 to 3.8%) and crude protein (13 to 13.5%) (Tovar et al. 2019), therefore, it can be considered as a promising carbon source. In the present work, a yield of 24.7% as AC has been obtained based on dry plant leaves. It is an expected result due to the most of the plant leaf content is water, in addition to drying of fresh leaves may not lead to complete drying of the plant leaves. By comparing our results with previous reports (Table 1), which adopted plant leaves with relatively low moisture content, it can be said that *Pontederia crassipe* leaves are promising carbon source. In general, the findings obtained from the present study suggest that the *Pontederia crassipe* leaves, can be obtained as an efficient and low cost biomass for the AC production with probable significant structural properties. Plant type and source species from which plant extract used for NPs synthesis also affects the size of fabricated NPs

Table 1 Percentage of AC yield and moisture content for some biomass sources adopted for the synthesis of AC.

Carbon source	Moisture % (wt)	AC yield % (wt)	Ref.
Pandanus odorifer leaves	28-30	25.7	(Fillaeli et al. 2019)
Vitis vinifera leaves	8.19	58.4	(Adetunji et al. 2020)
Dipterocarpus alatus Leaves	12	16.25	(Warangkana et al. 2021)
Typha orientalis leaves	2.5	39.22	(Anisuzzaman et al. 2015)
Pontederia crassipe leaves	5-7.2	24.7	present work

Characterization

FTIR analysis

FT-IR analysis was carried out in order to investigate the functional groups and chemical composition of synthesized nanomaterials. As Fig. 2(a) shows, the FTIR spectra of synthesized NPs were analyzed in the range 500 – 4000 cm^{-1}. The FT-IR spectrum of unmodified ZnO sample exhibits bands centered at 495 cm^{-1}, 1112 cm^{-1} and 1518 cm^{-1}. The band at 495 cm^{-1} is assigned to Zn-O bond vibration mode, which indicates the success of the green synthesis of ZnO NPs (Ameen et al. 2021). The band centered at 1112 cm^{-1} may be due to the presence C-O stretching bond of the aromatic rings related to phenols and flavonoids molecules present in the *Pontederia crassipe* leaves extract

(Alamdari et al. 2020). The band appeared at 1518 cm^{-1} suggests the presence of trace phytochemicals loaded onto ZnO surface which acted as reducing, stabilizing and capping agents, which may be correspond to –C–N-stretching vibration of amides or –C–O– stretching of alcohols and carboxylic acids which adsorbed on ZnO(Sana et al. 2020). The broad band around 3150- 3600 cm^{-1} indicate the presence of an O-H groups for the extract and ZnO which are assigned to the O-H stretching of phenolic and flavonoid compounds found in plant extract and, which was adsorbed on the ZnO surface (Barzinjy et al. 2020). It can be concluded from the FTIR analysis that the main oxygen containing groups are obviously present in the FTIR spectrum of ZnP NPs. The obtained FTIR spectrum of AC sample shows few bands, where most of the functional groups related to leaves phytochemicals were diminished during carbonation process which indicates the high purity of synthesized AC sample. This suggests that the thermal treatment led to the pyrolysis of most of the adsorbed biomolecules. The bands centered at 1452 and 1463 cm^{-1} indicate C=C bonds present in activated carbon (Xu et al. 2014). For AC/ZnO (5%) sample, notable peaks can be observed in range of 3100–3450 cm^{-1} indicating the existence of the O–H groups. Band at 470 cm^{-1} is clearly exhibited the existence of Zn-O bond. For ZnO/AC (10%) sample, it was noticed that the intensity of bands increased compared to ZnO/AC (5%) sample, with a slight shift towards the lower wavenumbers.

XRD analysis

In order to confirm the formation of the ZnO, AC and ZnO/AC NPs, XRD patterns were examined for synthesized materials. Additionally, XRD powder technique was employed to provide sufficient information about elemental analysis as well as for phase analysis. The XRD analysis is shown in Fig. 2(b). In XRD pattern of AC, a broad peak can be observed at $2\theta=24.11^0$ correspond to the 002 plane of carbon that assigned to the amorphous structure (Song et al. 2013). The intensity and position of peak indicate the low degree of graphitization. This indicates that the heating of biomass at high temperature causes the pyrolysis of organic substances into volatile products, which means that most of the non-carbon elements such as hydrogen, nitrogen and oxygen are removed in gaseous forms and leave a solid residue enriched with carbon. The peak centered at 24.11°, is possibly confirms that the activation and carbonization of *Pontederia crassipe* leaves powder significantly produce amorphous carbon. The XRD pattern of ZnO NPs pattern showed nine sharp and intense peaks centered at 2θ centered at 31.395°, 34.42°, 36.62°, 47.43°, 56.71°, 63.27°, 68.26° , 69.23° and 77.24° which were corresponded to crystal planes of (100), (002), (101), (102), (110), (103), (200), (112) , (201) and (202), respectively (Khashan et al. 2021). The XRD of ZnO NPs exhibited a single phase with clear diffraction peaks, which could be corresponded to hexagonal ZnO wurtzite phase (JCPDS Card no. 36–1451). Similar results were previously reported (Naseer et al. 2020), which revealed that the

biosynthesized ZnO NPs using *Cassia fistula* and *Melia azedarach* leaf extracts exhibited the hexagonal ZnO wurtzite phase. It also confirms that there is no characteristics XRD peaks due to any other materials or phases confirming the synthesized ZnO sample was free of impurities. These findings indicate that the *Pontederia crassipe* leaves extract offered efficiency and simplicity in the biosynthesis of ZnO NPs. The same peaks were observed in the ZnO/AC patterns, with the exception of those related to AC, which have completely disappeared, which may be due to low carbon content related to amorphous structure. Accordingly, no shift of the ZnO peaks was observed after activated carbon loading. The crystalline sizes of synthesized NPs were determined from Scherrer's equation:

$$\mathbf{D= 0.9\lambda/\beta\cos\theta} \quad (3)$$

Where D is the mean crystallite size in terms of nm, λ is the monochromatic wavelength of Cuk_{α} radiation (1.5406 nm), and β is the full width at half-maximum, θ is the he diffraction angle. The crystalline sizes of all synthesized sample calculated from Scherer's equation are shown in Table 2.

Table 2. The average crystallite size of ZnO, AC, ZnO/AC(5%) and ZnO/AC(10%) samples.

Samples	2θ	FWHM	D(nm)
ZnO	55.1962	0.6236	40.6372
AC	28.2487	7.5522	19.2425
ZnO/AC(5%)	54.7401	1.4013	37.6618
ZnO/AC(10%)	47.9775	3.8799	37.9064

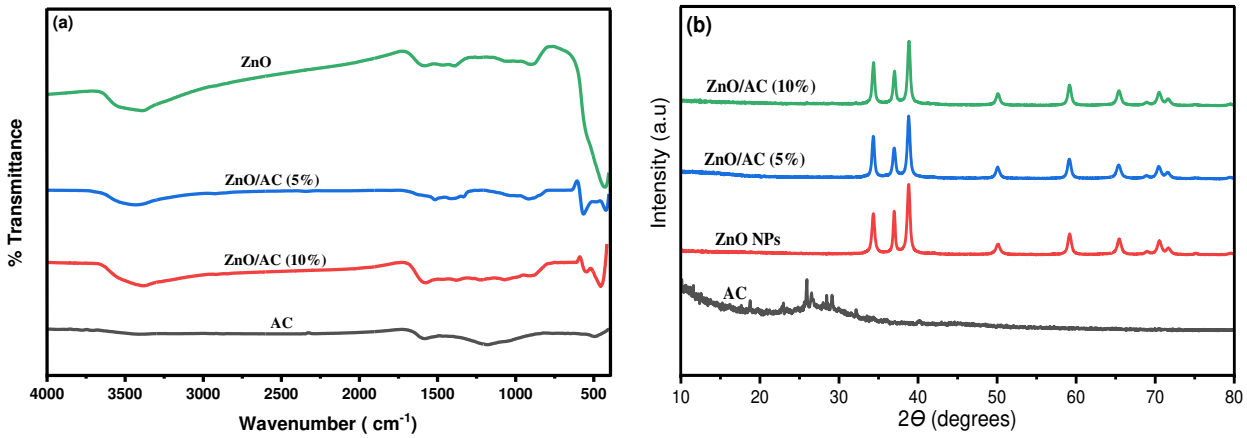

Fig. 2. FT-IR spectra (a) and XRD patterns (b) of ZnO, AC, ZnO/AC (5%), and ZnO/AC (10%) NPs.

BET/BJH analysis

BET/BJH analyses were conducted to investigate the textural properties of the as synthesized NPs. The specific surface area ($a_{s,BET}$) of fabricated nanopowders was examined employing BET analyzer via N_2 adsorption–desorption isotherms at 77 K and the results are shown in Fig. 3. In addition, pore size distribution was obtained from BJH method and the results are shown in Fig. 3. The specific surface area, isotherm type, pore volume, and hysteresis loop of four synthesized materials are listed in Table 3. BET-N_2 adsorption/desorption curves reveal that ZnO, AC, ZnO/AC (5%) and ZnO/AC (10%) have a surface area of 20.515, 753, 67.75 and 140.2 m²/g respectively. The high specific surface area of AC *Pontederia crassipe* leaves makes it an effective material in the adsorptive removal of various inorganic and organic pollutants from aqueous media. Moreover, simultaneously, the surface functionalization and activation processes of carbonaceous material generate a porous material. The lower specific surface area of ZnO NPs may be attributed to agglomeration of nanoparticles. From N_2 adsorption-desorption isotherms, it can be observed that four samples show typical III curve with type H3 hysteresis loop according to the IUPAC classification(Endres et al. 2021), indicating that the samples have a mesoporous texture. These findings indicate that AC derived from *Pontederia crassipe* leaves possesses a significant pore volume properties. Thus, utilizing cheap natural source, AC with high porosity and valuable surface texture was produced. BJH pore diameters found to be 4.12, 5.97, 12.63 and 7.59 nm for ZnO, AC, ZnO/AC(5%), and ZnO/AC(10%), respectively, which demonstrates that the all samples comprise of mesoporous surface according IUPAC definition. Because of their significant porous structure and surface area, green synthesized AC/ZnO samples produced by pyrolysis of *Pontederia crassipe* leaves and green fabrication of ZnO NPs may possess a promise activity for removal of organic dyes from aqueous solutions. It is generally believed that the controlling of thermal pyrolysis of cellulose, lignin and hemicellulose compounds contained in plant biomass can enhance the pore volume, porosity, and specific surface area, resulting in the formation of porous structure in the activated carbon (Mathangi et al. 2021). In general, it seems that porous surfaces were formed by carbonization process, which was also confirmed by morphology investigations.

Table 3. BET and BJH data of ZnO, AC, ZnO/AC(5%), and ZnO/AC(10%) samples.

Physicochemical properties	ZnO	AC	ZnO/AC (5%)	ZnO/AC (10%)
BET Surface Area, m^2/g	20.515	753	67.75	140.2
BJH surface area , m^2/g	11.361	299.63	42.76	75.42
Pore Volume, cm^3/g	0.02116	1.1243	0.2141	0.2707
Mean pore diameter , nm	4.1258	5.9707	12.63	7.59

Isotherm type	III	III	III	III
hysteresis loop	H3	H3	H3	H3

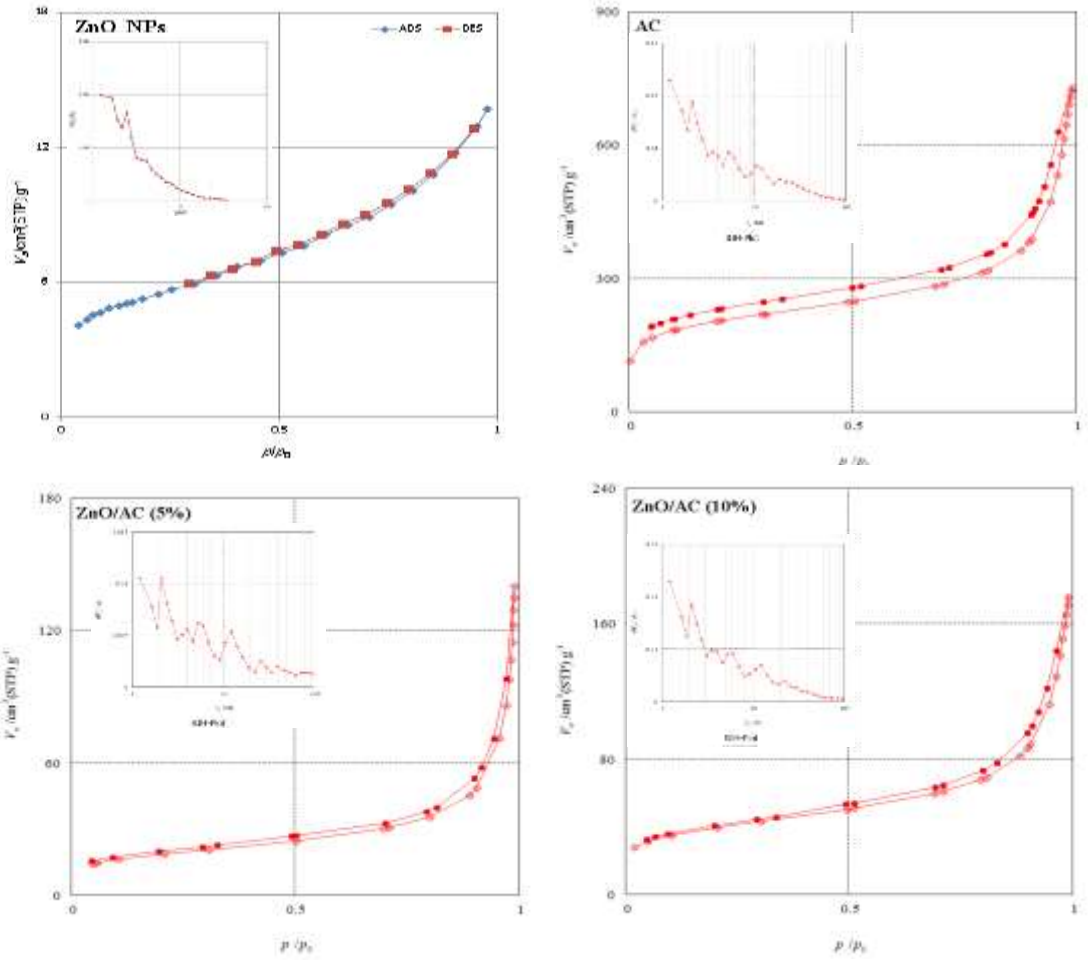

Fig 3. N_2 sorption isotherms of ZnO, AC, ZnO/AC (5%), and ZnO/AC (10%) NPs.

FESEM and EDX analysis

Investigation of surface morphology and particle distribution of as synthesized nanomaterials were studied by FE-SEM micrographs and EDX spectra. Fig. 4 illustrates the FE-SEM micrographs of ZnO, AC, ZnO/AC (5%) and ZnO/AC (10%) samples. Based on the FE-SEM analysis, most of the ZnO NPs were appeared to be uniform quasi-spherical-like morphology with a heterogeneous distribution due to occurrence significant aggregations in cluster forms. From FE-SEM analysis, it can be clearly noticed that the sizes of particles are in order of few tens of nanometers. These results agree with the findings of Fouladi-Fard et al. (2022), who confirmed that the utilize *Crataegus monogyna* extract produced ZnO NPs in spherical shapes (Reza et al. 2022). Reducing, capping and stabilizing of ZnO NPs utilizing the biomolecules contained in *Pontederia crassipe* leaves extract making them less agglomerated and more homogeneous. The FE-SEM image of AC revealed that the spherical morphology of sample has almost a similar particle size, which means that the chemical activation and

thermal treatment maintained the regular spherical shapes of carbon particles. In addition, the FESEM micrograph of AC sample show the formation of a porous surface. The FE-SEM images of the ZnO/AC samples indicate a wide distribution of particle sizes and showed irregular granular and spherical like shapes. However, by comparing between two ZnO/AC composites, it appears that ZnO/AC (10%) has lower particle sizes, which due to the high carbon content, which will form nuclei for the growth of ZnO NPs. Thus, ZnO/AC (5%) sample possesses higher particle sizes and have significant agglomerations due to loading of ZnO NPs onto lower carbon particles. The major benefit of biosynthesis process using plant extract is the variance of nanoparticle morphologies which may be depends on the plant extract utilized, as well as the its biomolecules content. The formation and purity of fabricated nanomaterials was confirmed by EDX spectrometry and Fig. 5 shows the EDX spectra of synthesized samples. The results reveal that peaks are assigned to ZnO, AC and ZnO/AC samples. The gold peak other than the zinc, oxygen, and carbon correspond to the gold grid, which is used for FESEM sample preparation. The EDX analysis indicated that the desired phase of Zn, O and C is existing in the samples and confirmed good purity for the fabricated NPs. Based on the FESEM images, the histograms of particle size distribution were performed, where the particles sizes of ZnO, AC, ZnO/AC(5%) and ZnO/AC(10%) were determined to be about 4.76, 12.11, 8.55, and 2.16, respectively. The ZnO EDX spectrum indicated the successful synthesis of ZnO NPs and the trace ratios of the other elements are due to the extract content. Our results are in agreement with those reported by (Venkateasan et al. 2017), who used *Ipomoea pescaprae* leaves extract for biosynthesis of ZnO NPs.

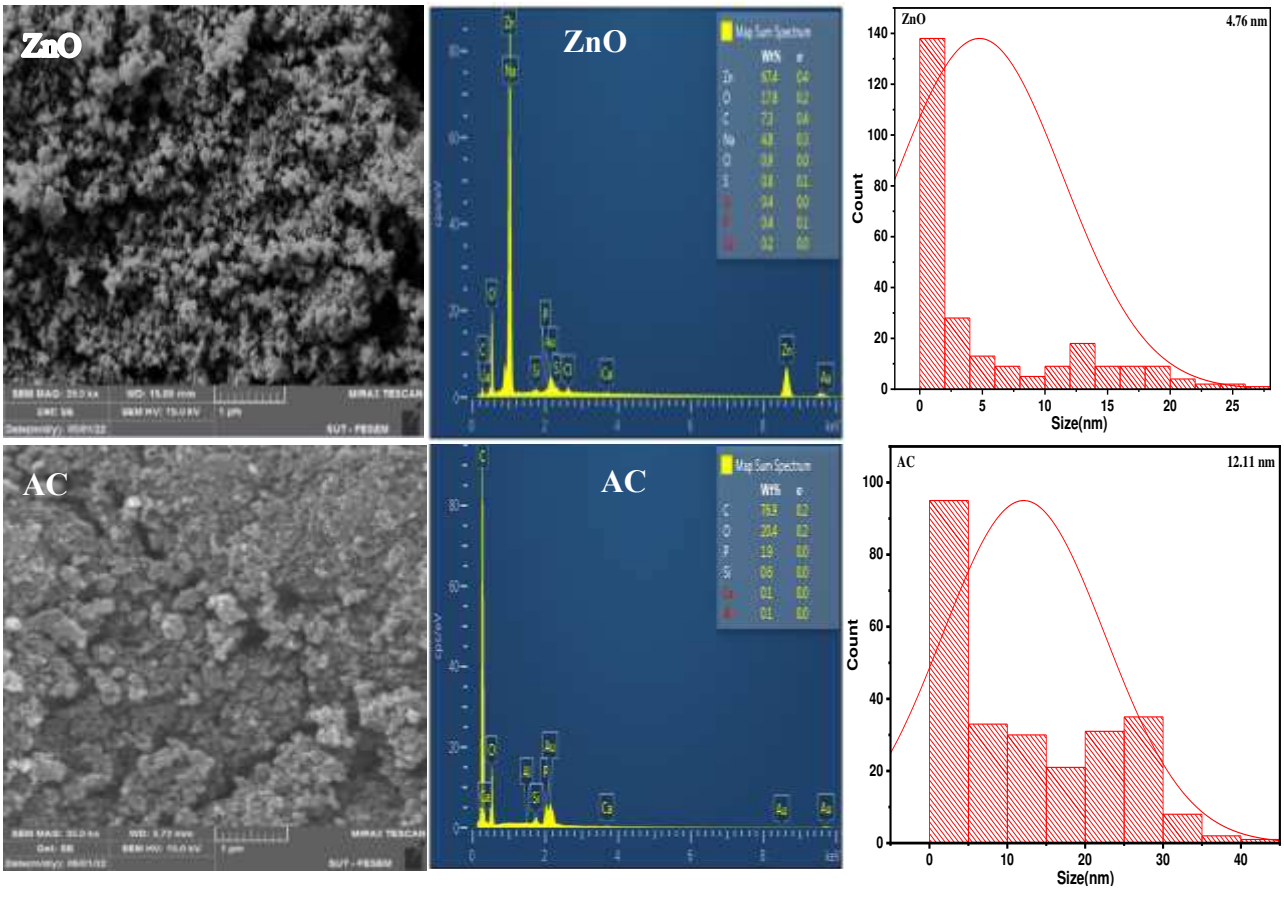

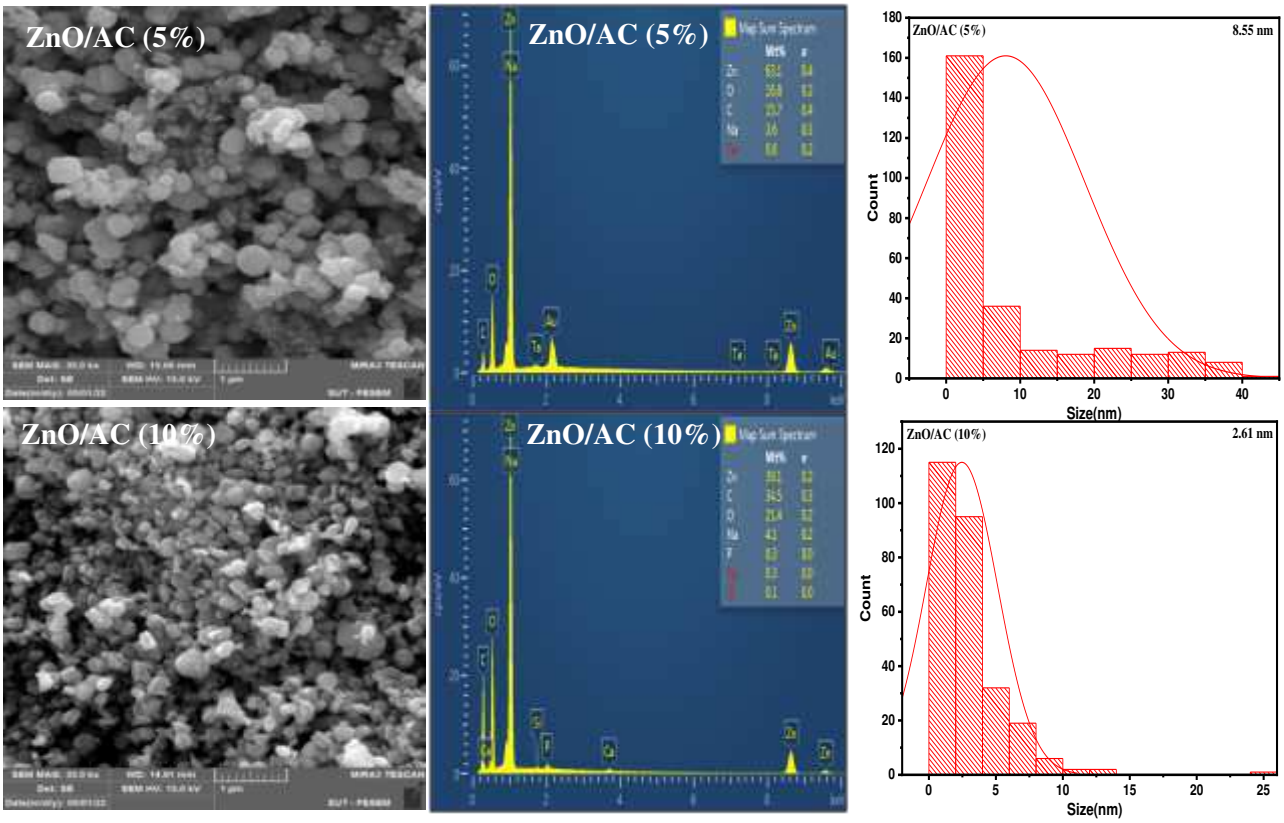

Fig.4. FESEM micrographs, EDS spectra and histograms of ZnO, AC, ZnO/AC(5%), and ZnO/AC(10%) samples.

TEM analysis

The morphology and dispersion of as synthesized materials were investigated using TEM analysis and the TEM images are shown in Fig.5. As clearly seen in its TEM image, ZnO NPs had spherical shapes to quasi-spherical ones. For the pure activated carbon, small, and almost disorder disperse spheres were obtained. In addition, the large number of white spots between the disordered carbon layers suggests that activated carbon possesses porous structures. In general, such disordered nature in carbon AC exhibits highly surface area which may be supported by Raman spectroscopy. The images clearly present a nanostructures consisting of ZnO NPs homogeneously dispersed on AC NPs, especially in the case of ZnO/AC(10%). After loading, the ZnO NPs remain homogeneously dispersed around the porous AC structure. In General, the TEM analyses show significant agglomerations/aggregations in ZnO/AC NPs which may be due to treatment of nanocomposites at high thermal conditions. It has been proven previously, the high surface energy resulted in increasing of particle size, and hence, at high temperature in aqueous media, the particles tend to have significant agglomerations (Endres et al. 2021). Thus, larger spheres are expected to be formed in

ZnO/AC (5%). These findings are obviously show that ZnO NPs are successfully loaded and stabilized onto porous activated carbon NPs.

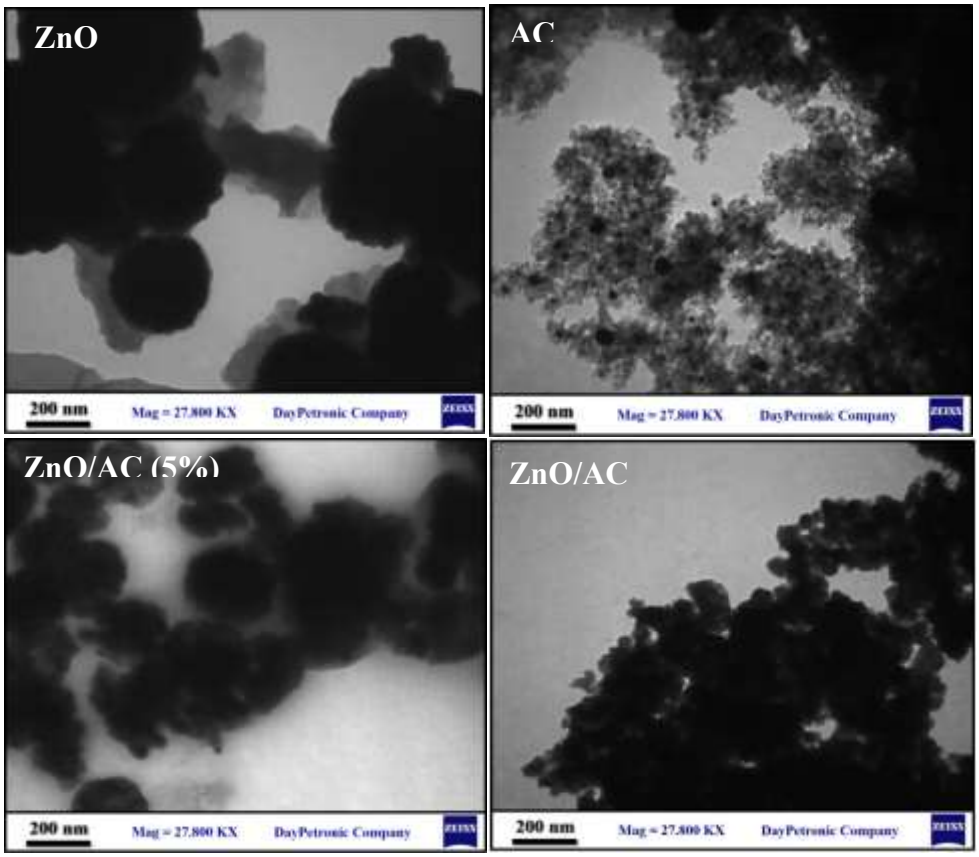

Fig. 5. TEM images of ZnO, AC, ZnO/AC(5%) and ZnO/AC(10%) NPs**.**

Raman spectroscopy

Raman spectroscopy is a useful tool that has been widely utilized to identify the chemical structure and crystalline nature of the synthesized nanomaterials. Fig. 6 displays the Raman spectra of the ZnO NPs, AC NPs and ZnO/AC nanocomposites. Since Raman spectrum of AC shows characteristic peaks are 1350 cm^{-1} (D band) and 1561 cm^{-1} (G band), this confirms the successful synthesis of AC. The Raman spectrum of ZnO/AC(5%) nanocomposites showed two peaks of high intensity at around 1319 cm^{-1} (D band) referred to as disordered carbon (sp^3) and 1561 cm^{-1} (G band) referred to as graphitic carbon (sp^2) belong to AC. On the other hand, ZnO/AC (5%) sample has D band at 1301 cm^{-1} and G band at 1530 cm^{-1}. A significant decline in the intensity of AC peaks was noticed in the prepared ZnO/AC nanocomposites with a decrease in the AC ratio. This confirms the properly and facility of the fabrication process adopting thermal route. The intensity ratio (I_D/I_G) can be used to investigate the disorder and order crystal structures. The spectral position of D and G bands an I_D/I_G are summarized in Table 4. The I_D/I_G ratios are 1.14, 1.12 and 1.11 for AC, ZnO/AC(10%), and ZnO/AC(5%) , respectively. In this manner, the higher I_D/I_G ratio of AC suggests

an increase of disordered carbon (sp^3) in comparison with graphitic carbon (sp^2). The results of the current study indicate that crystalline graphite derived from *Pontederia crassipe* leaves is lower than disordered graphite phase, so it does for *Clivia miniata* leaves (Gao et al. 2022). The difference in the intensities of D and G bands in the synthesized nanoparticles can mainly be due to the change in the mass of AC and to the loading of ZnO NPs, which act as defects on the AC surface and maintain their structural perfection after the anchoring of ZnO. It is reported that the carbonization temperature has a crucial effect on the graphitization degree and defects content, as the increase in temperature decreases the graphitization degree and the defects number increases (Yuan et al. 2021).

Table 4. Raman spectra information for AC, ZnO/AC(5%) and ZnO/AC(10%) samples.

Comp.	D-Band cm^{-1}	G-Band cm^{-1}	I_D/I_G
AC	1350	1561	1.14
ZnO/AC (5%)	1319	1561	1.11
ZnO/AC (10%)	1301	1530	1.12

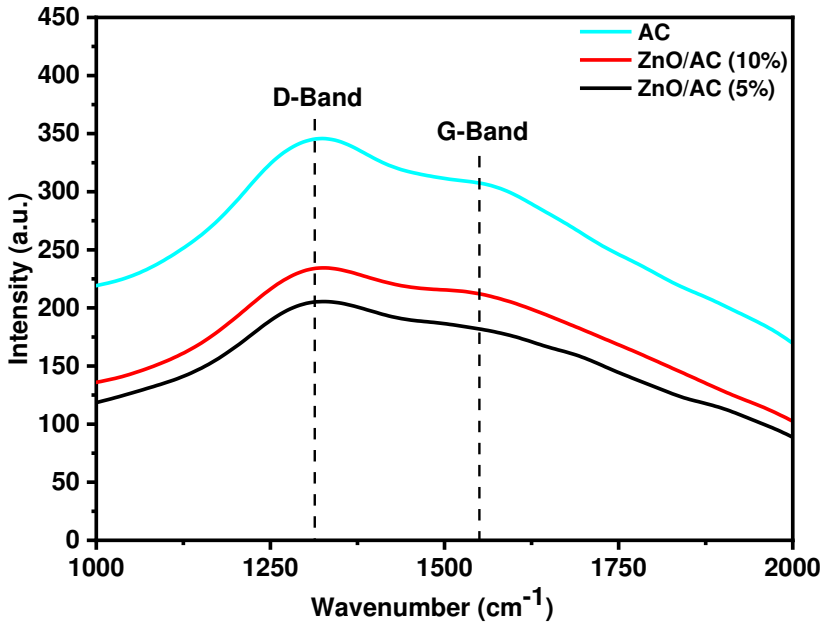

Fig. 6. Raman spectra of pure ZnO , AC, ZnO/AC(5%) and ZnO/AC(10%) NPs**.**

Adsorption of MG and CR by ZnO/AC (10%) NPs

Comparison of Adsorption Efficiency

Nowadays, continuous research is done to explore adsorbents with excellent adsorption capacity and low economic cost. The adsorption efficiency of synthesized nanomaterials was conducted depending on the contact time and the ratio of carbon content in synthesized nanocomposites. Due to the mentioned reasons, in the present study, the adsorption efficiency of ZnO, ZnO/AC(5%), and ZnO/AC(10%) nanocomposites was conducted in the CR and MG dyes uptake process from aqueous

solution and the results are displayed in Fig. 7a and b. As results revealed, the ZnO/AC(10%) nanocomposite presents the higher efficiency to remove CR and MG from aqueous solutions compared to pure ZnO and ZnO/AC(5%) , thus it can be adopted as an efficient adsorbent in the CR and MG dye adsorption process.

Effect of contact time

The influence of contact time on the adsorption of CR and MG using ZnO/AC(10%) sample in a time range of 0-120 min was studied in order to estimate the adsorption/desorption equilibrium time at pH 7, using 0.1 g/L ZnO/AC(10%), and CR(200 mg/L) and MG(100 mg/L) and the results are demonstrated in Fig. 7 a and b. It can clearly observed that the adsorption efficiency is strongly time dependent where the adsorption efficiencies of CR and MG dyes onto ZnO/AC(10%) were rapid at the first times and then it gradually slow down until it is fixed at a spesific value where no more dye molecules can adsorb on the surface. The results indicated that the equilibrium time for MG and CR removal on ZnO/AC(10%) NPs was determined to be 30 min. Clearly, at equilibrium time, the adsorption efficiency reached 75.09% for CR and 82.54% for MG. Since no alter in removal efficiency can be observed after this time. Subsequently, 30 min was fixed as an equilibrium time for further investigation of both dyes.

Effect of adsorbent amount

Adsorbent dosage is an important operational factor that influences the adsorption efficiency. The effect of ZnO/AC(10%) adsorbent dosage (0.01-0.2 g/L) on the removal of CR and MG ($[CR]_0$ = 200 mg/L, $[MG]_0$ = 100 mg/L) was investigated at 298K and pH of 7, and the results are clarified graphically in Fig. 7 c. In general, the results reveal that adsorption efficiency increases as the adsorbent mass increases. As results revealed, it can be seen that the ZnO/AC(10%) showed highest dye adsorption efficiency at 0.2 g/L. For the CR dye, the adsorption efficiency raised from 75.09% to 80.12% when the adsorbent dose increased from 0.1 to 0.2 g/L, respectively. For MG dye, in the same adsorbent dose range, the removal efficacy increased from 82.54% to 89.35%. This increment can be due to the more available active sites and higher adsorbing surface area for uptake of dye molecules at higher adsorbent ZnO/AC(10%). It is manifest from Fig. 7c that the stability of adsorption performance with rising absorption dose greater than 0.2 g/L can be due to the saturation of adsorption and may be due to the decrease in the accessible area of adsorbent particles and partial active sites blockage as a result of aggregation phenomena. Therefore, the utilise of ZnO/AC(10%) dose was specified at 0.2 g/L for both dyes because the removal efficiency is undetectable above this adsorbent dose. Comparable behaviour has been announced in previous works and it has been suggested that increasing the dose of adsorbents, beside to decreasing the efficient surface area, may be due to increasing the

diffusion path length, causes a decrease in the adsorption efficiency (Waheeb et al. 2020; Gurunathan et al. 2019).

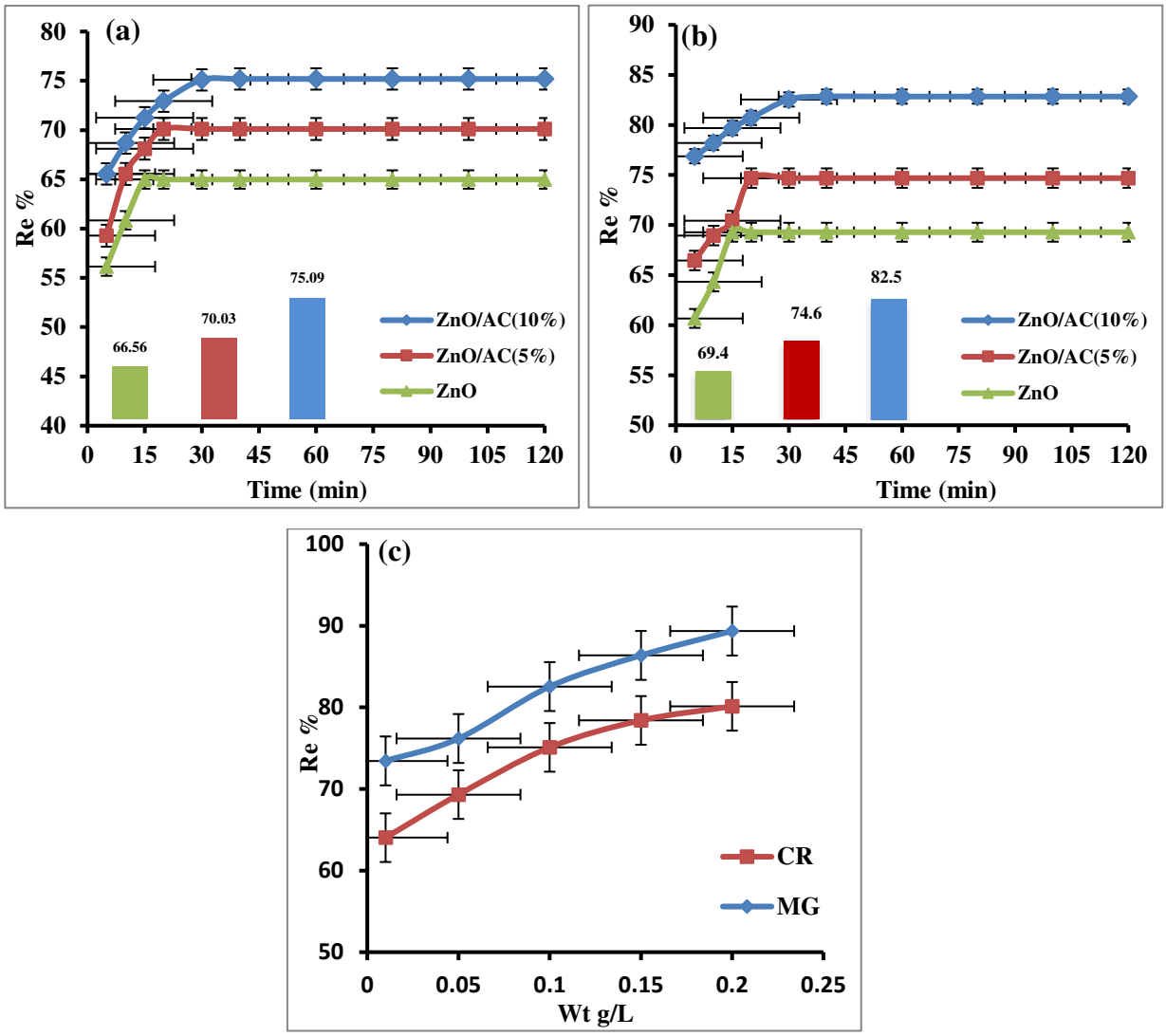

Fig. 7. Comparing of the effectiveness of synthesized adsorbents in adsorption of (a) CR and (b) MG. NPs ([CR] =200 mg/L, [MG]= 100 mg/L; adsorbent dose=0.1 g/L ; time=120 min ; pH =7 ; temperature= 298 K). (c) Effect of adsorbent dose on MG and CR adsorptive removal onto ZnO/AC(10%) NPs ([CR] =200 mg/L, [MG]= 100 mg/L; time=30 ; pH =7 ; temperature= 298 K).

Effect of pH

The solution pH plays a vital role in the removal water pollutants using adsorbents and catalysts. Adsorption experiments have been conducted at pH range 2-10 for CR and MG dyes, while the other operating factors were kept fixed. As elucidated in Fig. 8(a), CR adsorption decreases by increasing the pH value because it is a negatively charged dye. In contrast, a different behavior is observed by the MG dye because it is a positively charged dye. The higher CR removal efficiency was achieved to be 99.12%

at pH 2.0, on the other hand, the greater adsorption efficiency of MG dye was reached 99.81 at pH 8. For CR dye, on enhancement pH, the uptake efficiency was gradually declined. At pH 2, the ZnO/AC(10%) surface turns positively charged and adsorption is enhanced due to the electrostatic attraction forces negatively charged CR molecules and ZnO/AC surface. The decreasing in adsorption efficiency in alkaline solutions is attributed to competition between anionic CR molecules and hydroxyl anions to adsorb on the surface. Concerning the MG molecules, the adsorption behavior is reversed due to fact that the dye molecules possess positive charges. Fig. 8 clearly manifests that the high pH solutions improve MG dye adsorption and the low removal efficiencies of MG onto ZnO/AC(10%) were obtained at pHs 2 - 6 which might be attributed to the existence of excess H^+ cations that jostle the positive MG molecules to occupy the adsorption sites. At pH more than 8, the removal performance almost fixed due to the formation of soluble hydroxyl complexes (Emeniru et al. 2015). The adsorption behavior of both dyes can also be explained depending on the value of zero point charge (pH_{ZPC}) as shown in Fig. 8(b). The pH_{ZPC} was estimated to be 7.3, where at pH values lower than 7.3, the surface will have predominantly positive charges, which improves the adsorption efficiency of CR dye. Regarding the MG dye, it can be said that an increase of pH above 7.3 will provide a negatively charged surface, allowing better adsorption of the dye molecules. Generally, the findings exhibited that pH parameter has a different effect on the removal of water contaminations based on the nature of charges of adsorbent particles and pollutant molecules. **Accordingly, these findings indicate that the positive species present in the *Pontederia crassipe* leaves extract are adsorb onto AC/ ZnO surface that was prepared in an alkaline medium.**

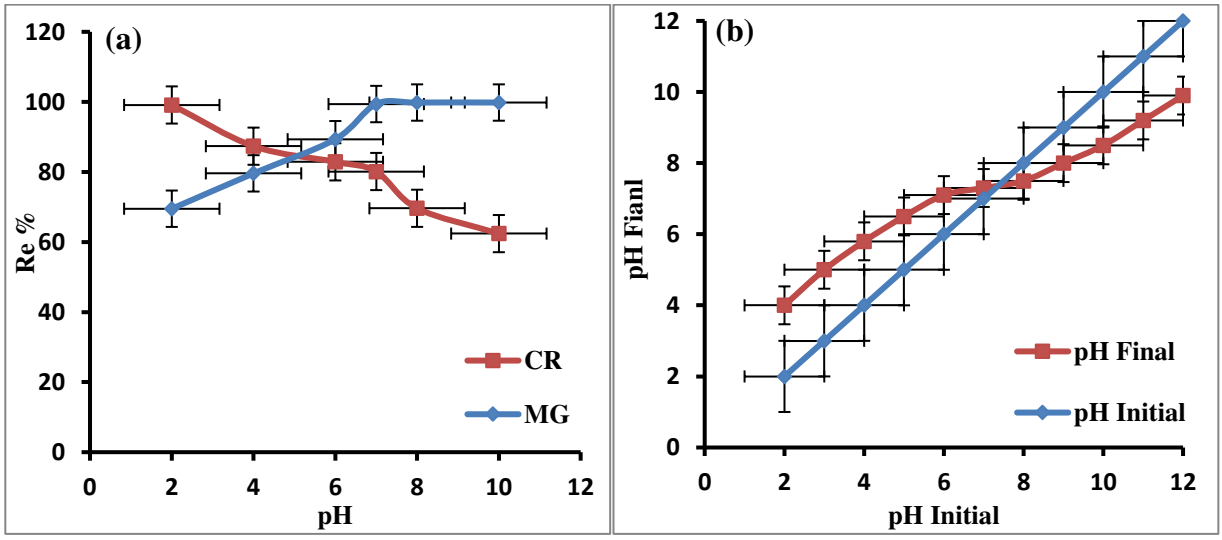

Fig. 8. Effect of pH on the CR and MG dyes adsorption over ZnO/AC(10%) NPs (a) and pH_{zpc} (b) ([CR] =200 mg/L, [MG]= 100 mg/L; adsorbent dose=0.2 g/L ; time=30 min ; temperature = 298 K).

.

Effect of ionic strength

Ionic strength is an important parameter influencing the removal of water pollutants, which might be employed to confirmation of the electrostatic interaction process for the removal of water contaminations. To study the influence of ionic strength on the adsorptive uptake of CR and MG dyes, various ionic strength ranging from 0.02 to 0.21 adopting NaCl, KCl, $MgCl_2$, and $CaCl_2$ electrolytes, have been investigated. The pH used during this experiment was kept constant at pH 7 for MG and 2 for CR. As Fig. 9 shows, the adsorption efficiency of both dyes decreased with the increase in electrolyte concentration. However, the increasing of electrolyte concentrations had high impact in decreasing MG adsorption, but this behavior is completely different for CR dye. The results of MG dye exhibited a decline in the removal activity depending on the size and charge of ions. As can be noticed, Mg^{2+} and Ca^{2+} ions have a negative effect on the adsorption efficiency more Na^{1+} and K^{1+} ions. As a result, ions with higher positive charges cause lower adsorption behavior compared to ions which have lower equivalent numbers. On the other hand, it seems that the decrease in the adsorption efficiency of the CR dye was greatly affected by the presence of Na^{1+} and K^{1+} ions. Generally, the likely reason behind the decreasing adsorption efficiency of MG dye at high electrolyte concentrations is the screening of electrostatic interaction of opposite charges by the electrolyte on the ZnO/ AC(10%) surface. As the results displayed, the adsorption efficiency of CR is inversely influenced, whether when changing the concentration and electrolyte type. The efficiency of MG dropped from its optimum value (99.81%) to the lowest one (79.83%) when utilizing $CaCl_2$ within the concentration range of 0.02-0.21N, while the removal of CR dye was not affected much at the same concentration range when using $MgCl_2$ and $CaCl_2$ salts.

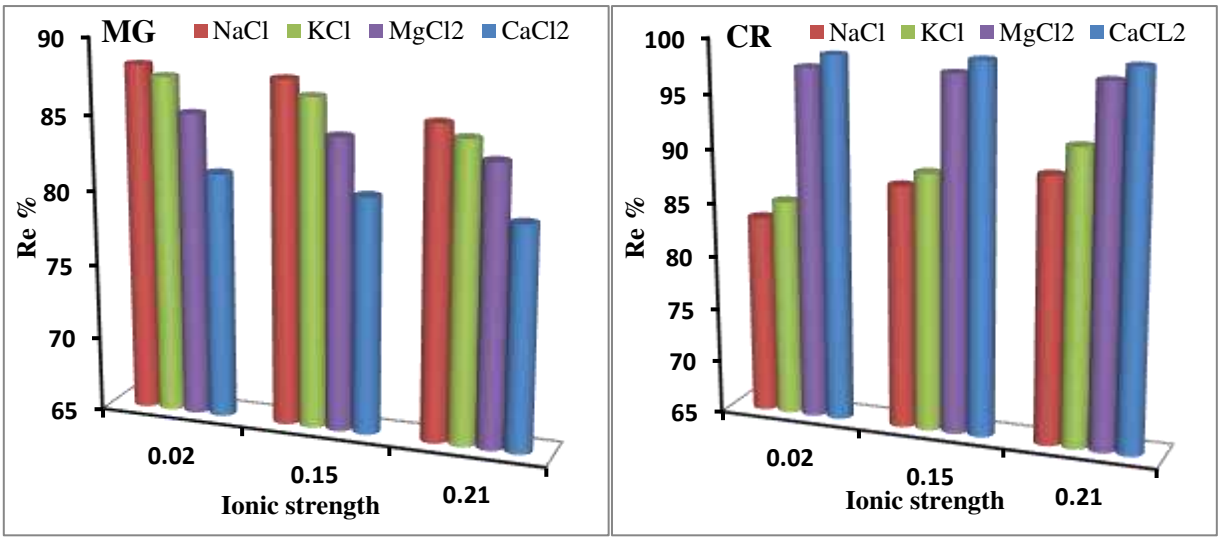

Fig. 9. Influence of ionic strength on the adsorption of MG and CR onto ZnO/AC(10%) NPs ([CR] =200 mg/L, [MG]= 100 mg/L; adsorbent dose= 0.2 g/L ; time=30 min ; pH=7 ; temperature, 298 K).

Thermodynamic study

Temperature is the most important factor in the adsorptive removal process of any substance onto various solid surfaces. The influence of the solution temperature on the adsorption of CR and MG by ZnO/AC(10%) was explored in the temperature range started from 288K in the multiples of 10K up to 318K, while other factors (contact time, adsorbent dosage, initial dye concentration, and solution pH) were kept constant. As shown in Fig. 10, the adsorption efficiency of MG was slightly influenced (2%) by the rising the solution temperature of the solution, where the increase in the temperature from 288 to 318 K accompanied with a very slight decrease in the MG removal from 99.7% to 99.8% exhibiting the adsorption process exothermic-nature. The increasing of adsorption efficiency of dye with rise in temperature is due to the increase in mobility of MG dye molecules as a result of increasing the average kinetic energies of the dye molecules by increasing the temperature (Wong et al. 2020). In contrast, when the temperature rose from 288K to 318K, the adsorption efficiency of CR is slightly decreased from 99.2% to 98.7%. Accordingly, studying the influence of the solution temperature on the adsorption performance will help in suggestion of interaction mechanism between adsorbate molecules and adsorbent surface, whether it is physisorption or chemisorption. Thermodynamic functions including the change in the enthalpy (ΔH^o), the change in the entropy (ΔS^o), and the change in the free energy (ΔH^o) were determined for the adsorption of CR and MG onto ZnO/AC(10%) at 288, 298, 308, and 318K employing equations (4) to (7) (Patel et al. 2020). Fig. 10 (a) shows the influence of temperature on the adsorption performance. Fig. 10(b) explores the relationship between $\ln K_{eq}$ and 1/T using Van't Hoff. The expressions of thermodynamic functions are expressed in following equations:

$$K_{eq} = \frac{Q_e \text{ x } m}{C_e \text{ x } V} \quad (4)$$

$$\Delta G^o = -RT ln K_{eq} \quad (5)$$

$$\ln K_{eq} = \frac{\Delta S^o}{R} - \frac{\Delta H^o}{RT} \quad (6)$$

$$\Delta S^o = \frac{\Delta H^o - \Delta G^o}{T} \quad (7)$$

where K_{eq} is the equilibrium absorption constant for the adsorption process, q_e is the amount of dye adsorbed in solution (mg g^{-1}), C_e is the equilibrium concentration of dye solution (mg/L), T is the absolute temperature (K), and R is the universal gas constant (R = 8.3144 J mol^{-1} K^{-1}). It is evident that

the results presented in Fig. 10 and Table 5 indicate that the MG dye uptake process is endothermic and spontaneous and the adsorption of CR dye is exothermic and spontaneous.

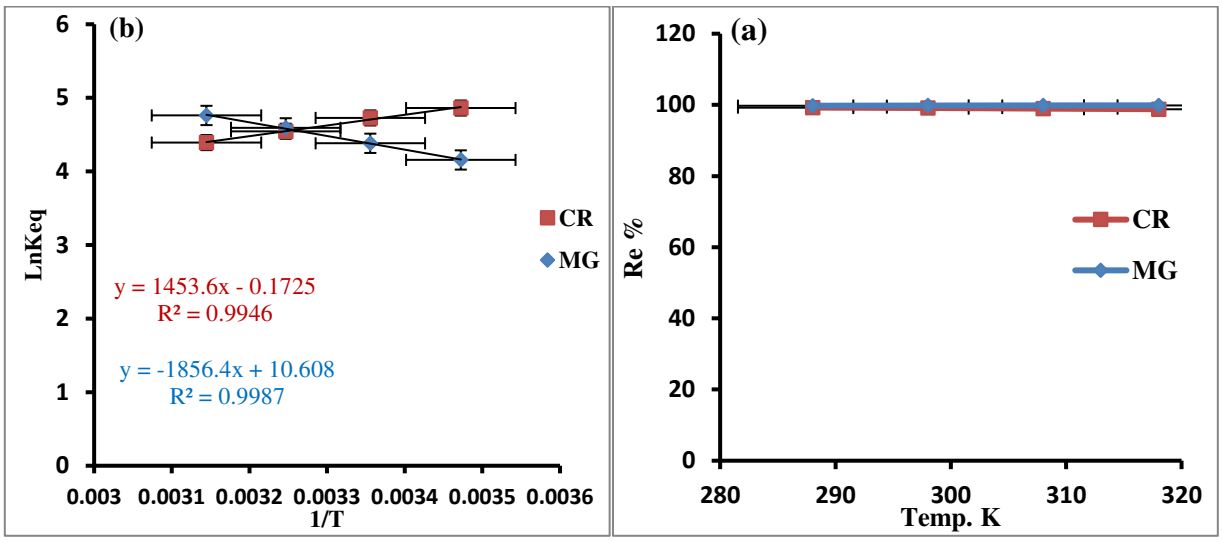

Fig. 10 (a) Effect of temperature on adsorption of CR and MG on ZnO/AC(10%) NPs and (b) Plot of Van't Hoff's equation ([CR] =200 mg/L, pH=2 (CR); [MG]= 100 mg/L ,pH=8 (MG) ; adsorbent dose=0.2 g/L ; equilibrium time=30 min).

Table 5. Thermodynamic results of the adsorption of CR and MG over AC/ ZnO NPs (10%).

Adsorbate	Temp. K	-ΔG° (kJ/mol)	ΔH° (kJ/mol)	ΔS° (J/mol k)
CR	288	11.6403	-12.0852	-1.54498
	298	11.7109		-1.25622
	308	11.6402		-1.44503
	318	11.6116		-1.4895
MG	288	9.95067	15.43411	88.14159
	298	10.8568		88.22448
	308	11.7588		88.28869
	318	12.5864		88.11472

However, positive ΔS^o value indicates an increase of degrees of freedom and occurrence of some structure changes in active sites of the adsorbent and refers to high rate random adsorption of dye molecules at the adsorbent-adsorbate interfaces.

Mechanism of adsorption

Generally, the interactions between the functional groups of adsorbent and adsorbate molecules are complicated. The adsorption behavior depends on the physicochemical nature of the adsorbent surface, the characteristics aqueous medium, and the chemical structure of the adsorbate. In general, the adsorption mechanisms onto adsorbent surface is divided into two types, physisorption and chemisorption. Accordingly, physisorption involves weak physical interactions (electrostatic, hydrogen bonding, and n-π stacking), while chemisorption which has a more prominent impact than physisorption, mostly includes surface complexation formation, chemical reduction and precipitation (Sabzehmeidani et al. 2021). Comparing the two types of adsorption, and chemisorption seems to be more efficient for the removal of various contaminations from different aqueous media. At certain particular conditions, the surface functional groups have remarkable effect on some mechanisms that involve surface complexation and electrostatic interaction. Based on the fact that ΔH^0 for physisorption adsorption ranges from 4 to 40 kJ/mol, compared to the chemisorption that involves higher bonding energy, which is more than 40 kJ/mol (Lafi et al. 2019). The findings of current work presented in Table 1 suggest that MG adsorption on ZnO/AC may be due to electrostatic interactions. Additionally, the ΔH^0 value for CR adsorption assumed that mechanism process of the removal of dye molecules onto ZnO/AC surface relates with the physisorption. Generally, in the aquatic media, the CR dye (CR-$SO_3^-Na^+$) would dissociate producing anion species (CR-SO_3^-) (Al-Harby et al. 2021). At acidic pH media, functional groups presented on ZnO/AC surface are strongly protonated leading to the surface getting positive charges, where below pH_{ZPC}, the ZnO turns into positive $ZnOH^{2+}$, and hence significant electrostatic interactions take place between CR-SO_3^- anions and the positively charged ZnO/AC surface (Degen et al. 2000). On the other hand, in a highly basic aqueous solutions, ZnO turns into $Zn(OH)_3^{1-}$ and $Zn(OH)_4^{2-}$ anions which the ZnO/AC surface possess negative charges, thus this might be accelerate the uptake of positively charged malachite MG cations ($^+$NH-MG). Due to low value of ΔH^0 for MG adsorption, electrostatic attraction might possibly occur between the positively charged $^+$NH-MG species and negatively charged ZnO/AC surface (Anfar et al. 2019).

.

Adsorption isotherms

Adsorption isotherms can provide some important data about the distribution of adsorption molecules between the solid and liquid phases, and can provide vital information about the interactions between the adsorbent and the adsorbent at a given temperature. In the current study, the results from the effect of dye concentration were adopted to estimate the nature of the removal by applying adsorption models, Langmuir, Fruendlich, and Temkin. Fig. 11 illustrates the nonlinear curves of adsorption isotherms of CR and MG dyes onto ZnO/AC(10%) NPs.

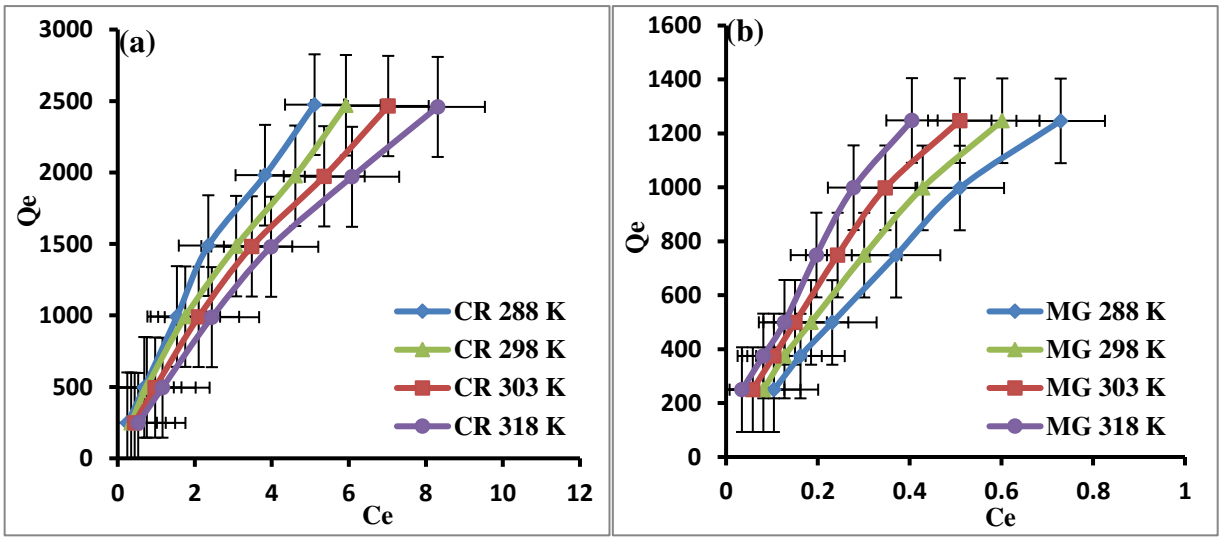

Fig. 11. Nonlinear curves of adsorption isotherms of CR and MG dyes onto ZnO/AC(10%) NPs, (adsorbent dose=0.2 g/L; time=30 min; [CR]= 50, 100, 200, 300, 400, and 500 mg/L, [MG]=50, 75,100,150, 200, and 250 mg/L, pH=2 (CR), MG pH=8 (MG)).

Langmuir isotherm

A study of the relationship between the adsorption capacity of the nano-adsorbents under study and the concentrations of organic dyes was carried out using the Langmuir adsorption equation. The Langmuir adsorption model is based on the premise that maximum adsorption corresponds to a saturated monolayer of molecules dissolved on the surface of the adsorbent with no side interaction at the surface between the adsorbent molecules. The linear expression of the Langmuir model is given by the following relationship (Langmuir 1918):

$$\frac{C_e}{Q_e} = \frac{1}{ab} + \frac{C_e}{a} \quad (8)$$

Where **a** is a maximum adsorption capacity (mg/g) corresponding to monolayer coverage and b is the Langmuir constant (mg/L). The Langmuir parameters were calculated from the slope and intercept of the Ce/qe line plots against the shape of C_e, and these parameters are shown in Table 5. The fundamental property of the Langmuir isotherm can be interpreted in terms of the dimensionless separation factor, R_L.

$$R_L = \frac{1}{(1+b\,C_o)} \quad (9)$$

The essential feature of the Langmuir isotherm is represented as a dimensionless separation factor R_L (Rahali et al.2021). The R_L value indicates that the type of isotherm is either undesirable ($R_L > 1$), desirable ($0< R_L < 1$), linear ($R_L = 1$) and irreversible ($R_L = 0$). The linear plot of Langmuir isotherm of CR and MG dyes is shown in Fig. 12(a, b).

Freundlich isotherm

The Freundlich model is an empirical expression employed to study heterogeneous systems, which suggests multilayer adsorption. The adsorption sites have non-uniform affinity for the adsorbate molecules and interactions in between sorbed molecules present. The linear form of this model is given by the following equation (Freundlich 1907):

$$Log\ Q_e = Log\ K_f + \frac{1}{n}\ Log\ \ C_e \quad (10)$$

Where K_f (L/mg) is the Freundlich isotherm constant, n is the adsorption parameter related to the adsorption intensity. 1/n e, the Freundlich model constant that expresses the adsorption capacity and intensity and gives an indication of the adsorption preference. The value of n, which is within the range from 1 to 10, indicates the interactions between the metal ion and the adsorbate. This parameter also expresses the type of adsorption. Accordingly, n values of 1 express linear adsorption, n values higher than 1 express physical and preferred adsorption, and n values less than 1 express chemical and preferred adsorption. The K_F and n values are calculated from the intercept and slope and the linear plot of Freundlich equation of CR and MG dyes is shown in Fig. 12(c, d).

Temkin isotherm

A Timken adsorption isotherm model is based on essential assumptions (i) the heat of absorption of all molecules in the layer decreases linearly with coverage due to the adsorbent-adsorbate interactions, (ii) the absorption is featuring by a homogeneous distribution of binding energies, which should strongly depend on the density, and the distribution of functional groups on the surface. The Temkin isotherm can be applied in the following linear relationship (Temkin et al. 1940):

$$Q_e = Bln\ A_t + B\ ln\mathrm{C_e} \quad (11)$$

Where A_t represents the equilibrium binding energy and constant B represents the adsorption heat. The linear plot of Temkin equation of CR and MG dyes is shown in in Fig. 12(e, f).

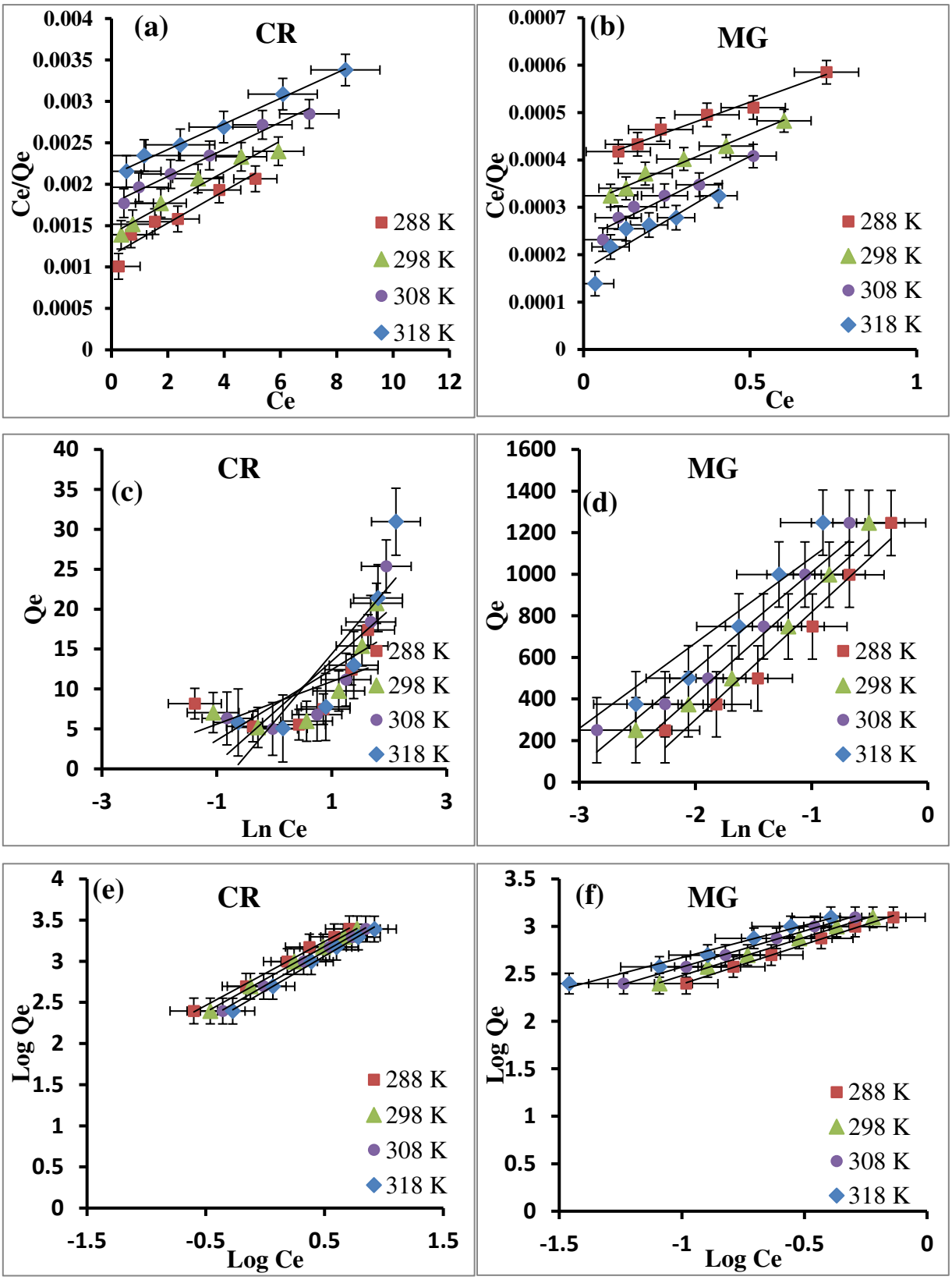

Fig. 12. The plot of linear formula of isotherms for CR and MG adsorption onto ZnO/AC(10%) NPs: (a,b) Langmuir,(c,d) Freundlich and (e,f) (adsorbent dose=0.2 g/L ; time=30 (min) ; pH=2 (CR), pH=8 (MG) ; temperature, 298 K).

Table 6. Parameters of adsorption isotherms.

Dye	Temp. K	Langmuir isotherm				Freundlich isotherm			Temkin isotherm		
		a (mg/g)	b (mg/L)	(R^2)	RL	(Kf)	(n)	(R^2)	B_T	A_T	(R^2)
CR	**288**	5000	0.1818	0.9102	0.0049	709.74	1.2861	0.997	2.6707	22.117	0.4144
	298	5000	0.1428	0.9617	0.0049	603.94	1.2545	0.9985	4.413	6.1274	0.6238
	308	5000	0.1111	0.9823	0.0049	506.4	1.2064	0.998	6.3996	3.0284	0.7002
	318	5000	0.0952	0.9928	0.0049	437.01	1.1856	0.9969	410.73	37.681	0.9046
MG	**288**	3333.3	0.75	0.9794	0.0131	1693.2	1.1951	0.9979	517.35	13.201	0.9663
	298	3333.3	1	0.988	0.009	1938.7	1.2404	0.9986	498.52	17.216	0.9658
	308	3333.3	1.5	0.9519	0.0066	2148.8	1.3144	0.9978	468.06	23.531	0.9544
	318	2500	2	0.8195	0.0049	2249.1	1.2403	0.9842	410.73	37.681	0.9046

After comparing the three isotherm models with the experimental data, especially correlation factor (R^2) presented in Table 6, it was clearly shown that the Freundlich isotherm represented the best fit for the adsorption experimental results over the other two isotherms,which indicates that the adsorption of CR and MG dyes over ZnO/AC(10%) surface is heterogeneous and multi-layered .In addition, these findings suggest the uniform distribution of functional groups both on the dye and adsorbent surface resulted in a uniform distribution of binding energies.

Kinetic study

The rate of uptake of dissolved dyes from the aqueous solution by solid adsorbents is important to analyze the adsorption kinetics using the theoretical models. In order to design and control the adsorption process and to investigate the adsorption rate the experimental data were subjected to pseudo first order and pseudo second order kinetic models. The expression for the pseudo-first-order rate, also known as Lagergren equation in following expression (Lagergren 1898):

$$\mathrm{Log}\,(q_e - q_t) = \log q_e - \frac{k_1 t}{2.303} \qquad (12)$$

Where adsorption capacity q_e (mg/g), and k_1 first order constants (min^{-1}). Plot of log (q_e - q_t) is represented as it is shown in Fig. 13(a) and the calculated data are listed in Table.6. The expression for the pseudo-second-order rate is shown by the following equation (Plazinski et al. 2013):

$$\frac{t}{q_t} = \frac{1}{k_2 q_e^2} + \frac{t}{q_e} \qquad (13)$$

Where: k_2 second order constants (g/mg min). Plot of t/q_t versus t is displayed in Fig. 13(b) and obtained data are shown in Table 7. These results confirm a better fit of the pseudo-second-order kinetic model for CR and MG dyes adsorption on ZnO/AC(10%) NPs.

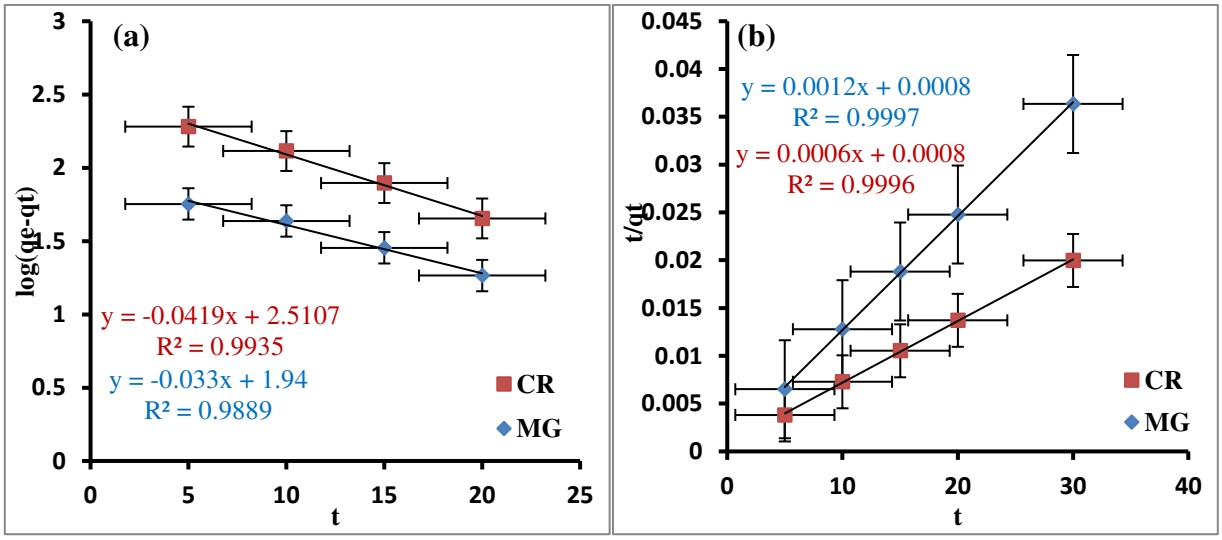

Fig. 13. Adsorption kinetics of CR and MG on ZnO/AC(10%) NPs (a) pseudo-first-order model and (b) pseudo second order model ([CR] =200 mg/L, [MG] = 100 mg/L; adsorbent dose=0.2 g/L ; time=30 (min) ; pH =7 ; temperature, 298 K).

Table 7. Kinetic parameters of CR and MG adsorption to ZnO/AC(10%) NPs.

Pseudo − first − order	$\mathbf{k_1}$	**qe**	$\mathbf{r^2}$
MG	0.0759	87.096	0.9889
CR	0.0964	324.12	0.9935
Pseudo − second − order	**k**	**qe**	$\mathbf{r^2}$
MG	0.0018	833.33	0.9997
CR	0.00045	1666.66	0.9996

Many works have been carried out to synthesis of activated carbon. Many studies on the modification of activated carbon with ZnO Nps have been conducted for the synthesis efficient adsorbents for removal various water contaminations. Table 7 lists a literature review based on ZnO/AC NPs as efficient adsorbents for removal organic dyes from aqueous media. Research conducted over the past few years has shown that ZnO/AC nanocomposites play an important role in

the environmental utilizations. As observed from Table 8, the adsorptive removal efficiency resulted from current study can be compared with those achieved from other adsorption studies. However, highly efficient adsorption and relatively cost effective make ZnO/AC suitable material for further adsorption studies. Furthermore, the facile and easy synthesis route, and enhanced efficiency of adsorption make synthesized ZnO/AC nanocomposites may be promising for further applications, such as photocatalysis, biological, medicinal and electronic studies.

Table 8 Adsorption efficiencies for CR by various adsorbents.

Adsorbent	**Synthesis Method**	**Pollutant/dye**	**Maximum Adsorption efficiency,%**	**Ref.**
ZnO/cotton stalks biochar	Precipitation	Congo red	89.65	(Iqbal et al.2021)
ZnO/AC	Precipitation	Malachite green	97.38	(Zaheer et al. 2019)
ZnO/MWCNTs	Precipitation	Congo red	99.8	(Arabi et al. 2019)
chitosan–zinc oxide	Precipitation	Malachite green	98.50	(Muinde et al. 2020)
ZnO/AC	precipitation	Malachite green	99	(Azad et al. 2015)
ZnO/AC	Thermal activation	Acid Black 1	92.88	(Afshina et al. 2021)
ZnO@Ananas comosus peel	Chemical reduction	Celestine blue	81.30	(Akpomie et al. 2020)
ZnO/AC	Precipitation	Chloroquine	78.89	(Dada et al. 2021)
ZnO/AC	Mixing	Reactive Blue 19	97.36	(Rashtbari et al. 2020)
ZnO/AC	precipitation	Congo red Malachite green	98.87 99.23	Present work

Analysis of dye/ZnO/AC(10%) samples

The used ZnO/AC(10%) surface was examined by FTIR, XRD, and FESEM techniques as shown in Fig. 14 a-d. Compared to pristine sample shown in Fig.2b, the XRD analysis confirmed that the ZnO/AC sample retained its chemical and crystalline structure. The FTIR spectra of MG/ZnO/AC and CR/ZnO/AC samples show some bands that are due to the adsorption of dye molecules onto adsorbent surface. On the other hand. As shown in Fig 14 c and d, the FESEM micrographs of adsorbent after it was utilized for dyes adsorption exhibited some changes in surface morphology. The FESEM micrographs of MG/ZnO/AC and CR/ZnO/AC samples show smoother surface morphology compared to FESEM analysis of adsorbent before adsorption (Fig. 4), which may be due to occupation of surface pores by dye molecules.

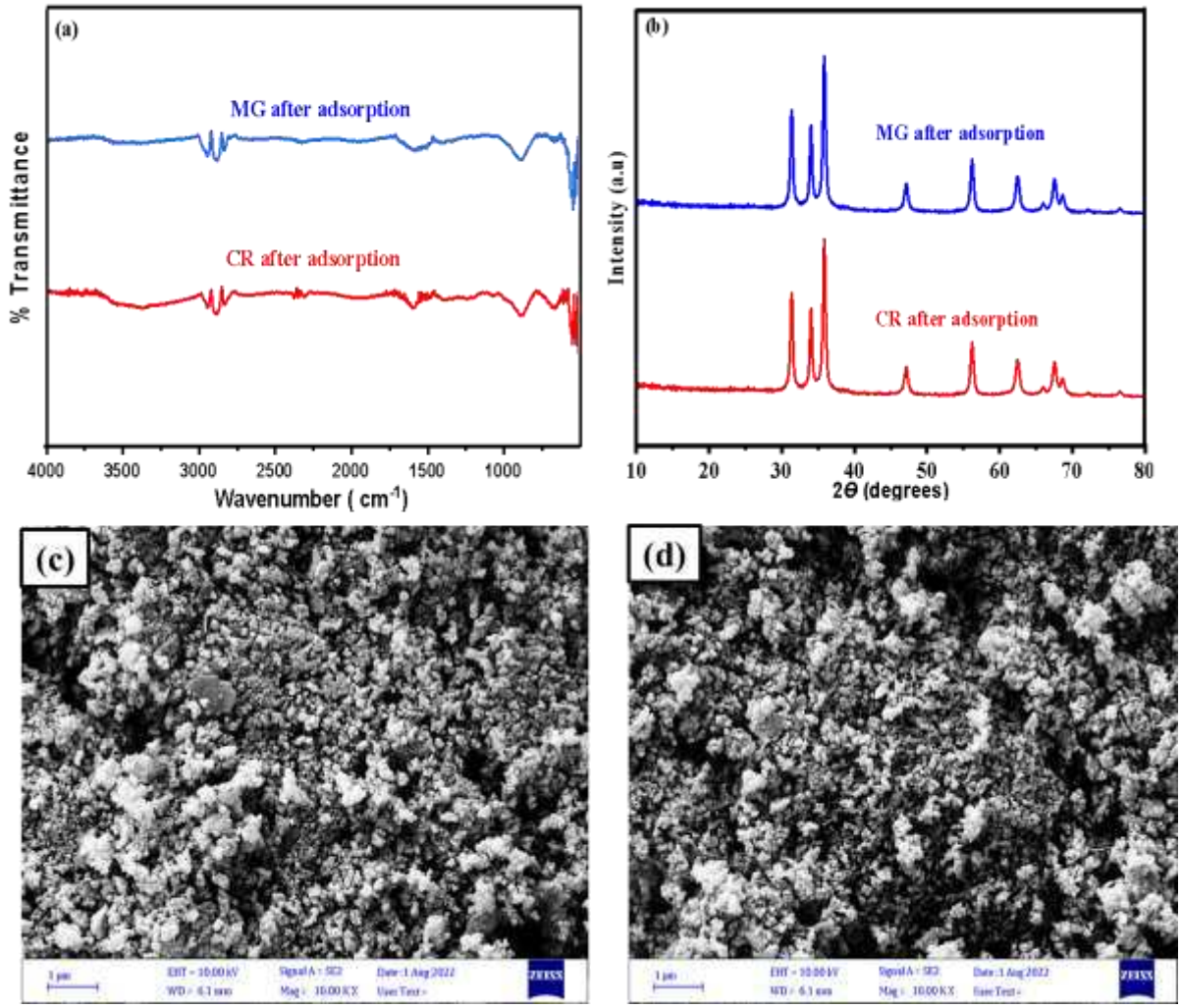

Fig. 14. (a) FTIR spectra, (b) XRD patterns, (c) FESEM micrographs of ZnO/AC(10%) sample after adsorption of CR dye and (d) FESEM micrographs of ZnO/AC(10%) sample after adsorption of MG dye

Conclusions

In general, ZnO and ZnO/AC nanoparticles were prepared by eco-friendly route and were analyzed by XRD, FTIR, FE-SEM, TEM, BET-BJH and Raman spectroscopy techniques with effective application as nanoadsorbents for the removal of CR and MG dyes from aqueous solutions. The results reveal that the as-synthesized samples are mostly assigned to spherical like structures. The obtained results showed that the sorption CR and MG dye over ZnO/AC(10%) was more efficient in comparison with bare ZnO. The ZnO/AC(10%) was found to enhance the removal of CR and MG at various contact times, adsorbent dosages, pH_s, solution temperatures, dye concentrations and ionic strengths. The adsorption efficiency of the ZnO/AC(10%) for CR and MG dye was reached 98.87% and 99.23%, respectively. Equilibrium data for CR and MG adsorption were best described by the e Freundlich isotherm and the rates of adsorptions for both dyes were determined to follow the pseudo second-order kinetic mode model. Negative $\Delta G°$ and Positive $\Delta H°$ values confined that the adsorptive removal of CR on The ZnO/AC(10%) was spontaneous and exothermic. On the other hand, adsorption of MG was found to be spontaneous and endothermic.

Funding Not applicable

Data availability The authors confirm that the data supporting the findings of this study are available within the article.

Declarations

Competing Interests The authors declare that they have no conflict of interest.

References

Abdelbaky, A. S., Abd El-Mageed, T. A., Babalghith, A. O., Selim, S., & Mohamed, A. M. (2022). Green synthesis and characterization of ZnO nanoparticles using Pelargonium odoratissimum (L.) aqueous leaf extract and their antioxidant, antibacterial and anti-inflammatory activities. *Antioxidants*, *11*(8), 1444.

Afshina, S., Poureshgha, Y., Rashtbaria, Y., Fazlzadehb, M., Aslc, F. B., Hamzezadeha, A., & Pormazard, S. M. (2021). Eco-friendly cost-effective approach for synthesis of ZnO nanoparticles and loaded on worn tire powdered activated carbon as a novel adsorbent to remove organic dyes from aqueous solutions: equilibrium, kinetic, regeneration and thermodynamic study. *Desalination and Water Treatment*, *227*, 391-403.

Ajel, M. K., & Al-nayili, A. (2022). Synthesis, characterization of Ag-WO3/bentonite nanocomposites and their application in photocatalytic degradation of humic acid in water. Environmental Science and Pollution Research, 1-15.

Akpomie, K. G., & Conradie, J. (2020). Synthesis, characterization, and regeneration of an inorganic–organic nanocomposite (ZnO@ biomass) and its application in the capture of cationic dye. *Scientific reports*, *10*(1), 1-12.

Alamdari, S., Sasani Ghamsari, M., Lee, C., Han, W., Park, H. H., Tafreshi, M. J., ... & Ara, M. H. M. (2020). Preparation and characterization of zinc oxide nanoparticles using leaf extract of Sambucus ebulus. *Applied Sciences*, *10*(10), 3620.

Alamdari, S., Sasani Ghamsari, M., Lee, C., Han, W., Park, H. H., Tafreshi, M. J., ... & Ara, M. H. M. (2020). Preparation and characterization of zinc oxide nanoparticles using leaf extract of Sambucus ebulus. *Applied Sciences*, *10*(10), 3620.

Albo Hay Allah, M. A., & Alshamsi, H. A. (2022). Green synthesis of ZnO NPs using Pontederia crassipes leaf extract: characterization, their adsorption behavior and anti-cancer property. *Biomass Conversion and Biorefinery*, 1-14.

Alhan, S., Nehra, M., Dilbaghi, N., Singhal, N. K., Kim, K. H., & Kumar, S. (2019). Potential use of ZnO@ activated carbon nanocomposites for the adsorptive removal of Cd2+ ions in aqueous solutions. *Environmental research*, *173*, 411-418.

Al-Harby, N. F., Albahly, E. F., & Mohamed, N. A. (2021). Kinetics, isotherm and thermodynamic studies for efficient adsorption of Congo Red dye from aqueous solution onto novel cyanoguanidine-modified chitosan adsorbent. *Polymers*, *13*(24), 4446.

Alwan, S. H., & Alshamsi, H. A. (2022). In situ synthesis NiO/F-MWCNTs nanocomposite for adsorption of malachite green dye from polluted water. *Carbon Letters*, 1-12.

Ameen, F., Dawoud, T., & AlNadhari, S. (2021). Ecofriendly and low-cost synthesis of ZnO nanoparticles from Acremonium potronii for the photocatalytic degradation of azo dyes. *Environmental Research*, *202*, 111700.

Aminu, I., Gumel, S. M., Ahmad, W. A., & Idris, A. A. (2020). Adsorption isotherms and kinetic studies of Congo-red removal from waste water using activated carbon prepared from jujube seed. *American Journal of Analytical Chemistry*, *11*(01), 47.

Anfar, Z., Zbair, M., Ahsaine, H. A., Abdellaoui, Y., El Fakir, A. A., Amaterz, E. H., ... & El Alem, N. (2019). Preparation and characterization of porous carbon@ ZnO-NPs for organic compounds removal: classical adsorption versus ultrasound assisted adsorption. *ChemistrySelect*, *4*(17), 4981-4994.

Anisuzzaman, S. M., Joseph, C. G., Daud, W. M. A. B. W., Krishnaiah, D., & Yee, H. S. (2015). Preparation and characterization of activated carbon from Typha orientalis leaves. *International Journal of Industrial Chemistry*, *6*(1), 9-21.

Arabi, S. M. S., Lalehloo, R. S., Olyai, M. R. T. B., Ali, G. A., & Sadegh, H. (2019). Removal of congo red azo dye from aqueous solution by ZnO nanoparticles loaded on multiwall carbon nanotubes. *Physica E: Low-Dimensional Systems and Nanostructures*, *106*, 150-155.

Awe, A. A., Opeolu, B. O., Fatoki, O. S., Ayanda, O. S., Jackson, V. A., & Snyman, R. (2020). Preparation and characterisation of activated carbon from Vitis vinifera leaf litter and its adsorption performance for aqueous phenanthrene. *Applied Biological Chemistry*, *63*(1), 1-17.

Azad, F. N., Ghaedi, M., Dashtian, K., Hajati, S., Goudarzi, A., & Jamshidi, M. (2015). Enhanced simultaneous removal of malachite green and safranin O by ZnO nanorod-loaded activated carbon: modeling, optimization and adsorption isotherms. *New Journal of Chemistry*, *39*(10), 7998-8005.

Bakrim, W. B., Ezzariai, A., Karouach, F., Sobeh, M., Kibret, M., Hafidi, M., ... & Yasri, A. (2022). Eichhornia crassipes (Mart.) Solms: A comprehensive review of its chemical composition, traditional use, and value-added products. *Frontiers in pharmacology*, *13*

Barzinjy, A. A., & Azeez, H. H. (2020). Green synthesis and characterization of zinc oxide nanoparticles using Eucalyptus globulus Labill. leaf extract and zinc nitrate hexahydrate salt. *SN Applied Sciences*, *2*(5), 1-14.

Bharti, J., Kumar, S. S., Kumar, V., Kumar, A., & Kumar, D. (2022). A review on the capability of zinc oxide and iron oxides nanomaterials, as a water decontaminating agent: Adsorption and photocatalysis. *Applied Water Science*, *12*(3), 46.

Bhuiyan, M. R. A., & Mamur, H. (2021). A Brief Review of the Synthesis of ZnO Nanoparticles for Biomedical Applications. *Iranian Journal of Materials Science and Engineering*, *18*(3), 1-27.

Chanikya, P., Nidheesh, P. V., Babu, D. S., Gopinath, A., & Kumar, M. S. (2021). Treatment of dyeing wastewater by combined sulfate radical based electrochemical advanced oxidation and electrocoagulation processes. *Separation and Purification Technology*, *254*, 117570.

Chen, Y., Zhang, X., Chen, W., Yang, H., & Chen, H. (2017). The structure evolution of biochar from biomass pyrolysis and its correlation with gas pollutant adsorption performance. *Bioresource technology*, *246*, 101-109.

Dada, A. O., Inyinbor, A. A., Bello, O. S., & Tokula, B. E. (2021). Novel plantain peel activated carbon–supported zinc oxide nanocomposites (PPAC-ZnO-NC) for adsorption of chloroquine synthetic pharmaceutical used for COVID-19 treatment. *Biomass Conversion and Biorefinery*, 1-13.

Daud, N. M., Abdullah, S. R. S., Hasan, H. A., & Dhokikah, Y. (2022). Integrated physical-biological treatment system for batik industry wastewater: A review on process selection. *Science of The Total Environment*, 152931.

Degen, A., & Kosec, M. (2000). Effect of pH and impurities on the surface charge of zinc oxide in aqueous solution. *Journal of the European Ceramic Society*, *20*(6), 667-673.

El-Bery, H. M., Saleh, M., El-Gendy, R. A., Saleh, M. R., & Thabet, S. M. (2022). High adsorption capacity of phenol and methylene blue using activated carbon derived from lignocellulosic agriculture wastes. *Scientific reports*, *12*(1), 1-17.

Elfeky, A. S., Youssef, H. F., & Elzaref, A. S. (2020). Adsorption of dye from wastewater onto ZnO nanoparticles-loaded zeolite: kinetic, thermodynamic and isotherm studies. *Zeitschrift für Physikalische Chemie*, *234*(2), 255-278.

Emeniru, D. C., Onukwuli, O. D., DouyeWodu, P. E., & Okoro, B. I. (2015). The equilibrium and thermodynamics of methylene blue uptake onto ekowe clay; influence of acid activation and calcination. *International Journal of Engineering and Applied Sciences*, *2*(5), 257933.

Endres, S. C., Ciacchi, L. C., & Mädler, L. (2021). A review of contact force models between nanoparticles in agglomerates, aggregates, and films. *Journal of Aerosol Science*, *153*, 105719.

Fillaeli, A., Kristianingrum, S., Siswani, E. D., & Fatimah, S. D. (2019). Synthesis activated carbon of screw-pine leaves by HNO3 and its properties. In *Journal of Physics: Conference Series* (Vol. 1156, No. 1, p. 012001). IOP Publishing.

Fouladi-Fard, R., Aali, R., Mohammadi-Aghdam, S., & Mortazavi-derazkola, S. (2022). The surface modification of spherical ZnO with Ag nanoparticles: A novel agent, biogenic synthesis, catalytic and antibacterial activities. *Arabian Journal of Chemistry*, *15*(3), 103658.

Freundlich, H. (1907). Über die adsorption in lösungen. *Zeitschrift für physikalische Chemie*, *57*(1), 385-470.

Gao, W. (2022). Porous Biomass Carbon Derived from Clivia miniata Leaves via NaOH Activation for Removal of Dye. *Materials*, *15*(4), 1285.

Gurunathan, P., Hari, S., Suseela, S. B., Sankararajan, R., & Mukannan, A. (2019). Production, characterization and effectiveness of cellulose acetate functionalized ZnO nanocomposite adsorbent for the removal of Se (VI) ions from aqueous media. *Environmental Science and Pollution Research*, *26*(1), 528-543.

Hamad, H. N., & Idrus, S. (2022). Recent Developments in the Application of Bio-Waste-Derived Adsorbents for the Removal of Methylene Blue from Wastewater: A Review. *Polymers*, *14*(4), 783.

Hammood, Z. A., Chyad, T. F., & Al-Saedi, R. (2021). Adsorption performance of dyes over zeolite for textile wastewater treatment. *Ecological Chemistry and Engineering*, *28*(3), 329-337.

Huang, R., Zhang, Q., Yao, H., Lu, X., Zhou, Q., & Yan, D. (2021). Ion-exchange resins for efficient removal of colorants in bis (hydroxyethyl) terephthalate. *ACS omega*, *6*(18), 12351-12360.

Hussain, N., Alwan, S., Alshamsi, H., & Sahib, I. (2020). Green synthesis of S-and N-codoped carbon nanospheres and application as adsorbent of Pb (II) from aqueous solution. *International Journal of Chemical Engineering*, *2020*.

Ibrahim, S. M., Hassanin, H. M., & Abdelrazek, M. M. (2020). Synthesis, and characterization of chitosan bearing pyranoquinolinone moiety for textile dye adsorption from wastewater. *Water Science and Technology*, *81*(3), 421-435.

Iqbal, M. M., Imran, M., Hussain, T., Naeem, M. A., Al-Kahtani, A. A., Shah, G. M., & Ali, S. (2021). Effective sequestration of Congo red dye with ZnO/cotton stalks biochar nanocomposite: MODELING, reusability and stability. *Journal of Saudi Chemical Society*, *25*(2), 101176.

Jan, H., Shah, M., Andleeb, A., Faisal, S., Khattak, A., Rizwan, M., ... & Abbasi, B. H. (2021). Plant-based synthesis of zinc oxide nanoparticles (ZnO-NPs) using aqueous leaf extract of aquilegia pubiflora: their antiproliferative activity against HepG2 cells inducing reactive oxygen species and other in vitro properties. *Oxidative medicine and cellular longevity*, *2021*.

Jayachandran, A., Aswathy, T. R., & Nair, A. S. (2021). Green synthesis and characterization of zinc oxide nanoparticles using Cayratia pedata leaf extract. *Biochemistry and Biophysics Reports*, *26*, 100995.

Kar, P., Jain, P., Gupta, R. K., & Tripathi, K. M. (2020). Emerging carbon-based nanocomposites for remediation of heavy metals and organic pollutants from wastewater. *Emerging Carbon-Based Nanocomposites for Environmental Applications*, 1-29.

Khalili, S., Khoshandam, B., & Jahanshahi, M. (2016). Synthesis of activated carbon/polyaniline nanocomposites for enhanced CO 2 adsorption. *RSC advances*, *6*(42), 35692-35704.

Khangwichian, W., Pattamasewe, S., Laungphairojana, A., Leesing, R., Hunt, A. J., & Ngernyen, Y. (2021). Preparation of activated carbons from hydrolyzed Dipterocarpus alatus leaves: value added product from biodiesel production waste. *Journal of the Japan Institute of Energy*, *100*(10), 219-224.

Khashan, K. S., Badr, B. A., Sulaiman, G. M., Jabir, M. S., & Hussain, S. A. (2021, March). Antibacterial activity of Zinc Oxide nanostructured materials synthesis by laser ablation method. In *Journal of Physics: Conference Series* (Vol. 1795, No. 1, p. 012040). IOP Publishing.

Kheddo, A., Rhyman, L., Elzagheid, M. I., Jeetah, P., & Ramasami, P. (2020). Adsorption of synthetic dyed wastewater using activated carbon from rice husk. *SN Applied Sciences*, *2*(12), 1-14.

Lafi, R., Montasser, I., & Hafiane, A. (2019). Adsorption of congo red dye from aqueous solutions by prepared activated carbon with oxygen-containing functional groups and its regeneration. *Adsorption Science & Technology*, *37*(1-2), 160-181.

Lagergren, S. (1898). Zur theorie der sogenannten adsorption geloster stoffe. *Kungliga svenska vetenskapsakademiens. Handlingar*, *24*, 1-39.

Lalitha, P., Sripathi, S. K., & Jayanthi, P. (2012). Secondary metabolites of Eichhornia crassipes (waterhyacinth): a review (1949 to 2011). *Natural product communications*, *7*(9), 1934578X1200700939.

Langmuir, I. (1918). The adsorption of gases on plane surfaces of glass, mica and platinum. *Journal of the American Chemical society*, *40*(9), 1361-1403.

Lellis, B., Fávaro-Polonio, C. Z., Pamphile, J. A., & Polonio, J. C. (2019). Effects of textile dyes on health and the environment and bioremediation potential of living organisms. *Biotechnology Research and Innovation*, *3*(2), 275-290.

Ma, H. T., Pham, N. B., Nguyen, D. C., Vo, K. T. D., Ly, H. C., & Phan, T. D. (2017). Effect of the carbonization and activation processes on the adsorption capacity of rice husk activated carbon. *Vietnam Journal of Science and Technology*, *55*(4), 485-493.

Maniarasu, R., Rathore, S. K., & Murugan, S. (2022). Preparation, characterization, and performance of activated carbon for CO2 adsorption from CI engine exhaust. *Greenhouse Gases: Science and Technology*, *12*(2), 284-304.

Martinez Stagnaro, S. Y., & Volzone, C. (2019). Adsorption of anionic dyes monoazo and diazo using organo-bentonites. *SN Applied Sciences*, *1*(1), 1-10.

Mathangi, J. B., Kalavathy, M. H., & Miranda, L. R. (2021). Pore Formation Mechanism and Sorption Studies Using Activated Carbon from Gleditsia triacanthos. *Chemical Engineering & Technology*, *44*(5), 892-900.

Mohd Yusof, H., Mohamad, R., Zaidan, U. H., & Rahman, A. (2019). Microbial synthesis of zinc oxide nanoparticles and their potential application as an antimicrobial agent and a feed supplement in animal industry: a review. *Journal of animal science and biotechnology*, *10*(1), 1-22.

Mok, C. F., Ching, Y. C., Muhamad, F., Abu Osman, N. A., Hai, N. D., & Che Hassan, C. R. (2020). Adsorption of dyes using poly (vinyl alcohol)(PVA) and PVA-based polymer composite adsorbents: a review. *Journal of Polymers and the Environment*, *28*(3), 775-793.

Mokif, L. A. (2019). Removal methods of synthetic dyes from industrial wastewater: a review. *Mesopotamia Environmental Journal (mesop. environ. j) ISSN: 2410-2598*, *5*(1), 23-40.

Muinde, V. M., Onyari, J. M., Wamalwa, B., & Wabomba, J. N. (2020). Adsorption of malachite green dye from aqueous solutions using mesoporous chitosan–zinc oxide composite material. *Environmental Chemistry and Ecotoxicology*, *2*, 115-125.

Naseer, M., Aslam, U., Khalid, B., & Chen, B. (2020). Green route to synthesize Zinc Oxide Nanoparticles using leaf extracts of Cassia fistula and Melia azadarach and their antibacterial potential. *Scientific Reports*, *10*(1), 1-10.

Nasrollahzadeh, M. S., Hadavifar, M., Ghasemi, S. S., & Arab Chamjangali, M. (2018). Synthesis of ZnO nanostructure using activated carbon for photocatalytic degradation of methyl orange from aqueous solutions. *Applied Water Science*, *8*(4), 1-12.

Nie, D., Wang, P., Zang, C., Zhang, G., Li, S., Liu, R., & Dai, J. (2022). Preparation of ZnO-Incorporated Porous Carbon Nanofibers and Adsorption Performance Investigation on Methylene Blue. *ACS omega*, *7*(2), 2198-2204.

Patel, H. (2020). Batch and continuous fixed bed adsorption of heavy metals removal using activated charcoal from neem (Azadirachta indica) leaf powder. *Scientific Reports*, *10*(1), 1-12.

Paton-Carrero, A., Sanchez, P., Sánchez-Silva, L., & Romero, A. (2022). Graphene-based materials behaviour for dyes adsorption. *Materials Today Communications*, *30*, 103033.

Plazinski, W., Dziuba, J., & Rudzinski, W. (2013). Modeling of sorption kinetics: the pseudo-second order equation and the sorbate intraparticle diffusivity. *Adsorption*, *19*(5), 1055-1064.

Powar, A. S., Perwuelz, A., Behary, N., Hoang, L., & Aussenac, T. (2020). Application of ozone treatment for the decolorization of the reactive-dyed fabrics in a pilot-scale process—optimization through response surface methodology. *Sustainability*, *12*(2), 471.

Purnaningtyas, M. A. K., Sudiono, S., & Siswanta, D. (2020). Synthesis of activated carbon/chitosan/alginate beads powder as an adsorbent for methylene blue and methyl violet 2B dyes. *Indonesian Journal of Chemistry*, *20*(5), 1119-1130.

Qin, Y., Wang, C., Sun, X., Ma, Y., Song, X., Wang, F., ... & Ning, P. (2021). Defects on activated carbon determine the dispersion of active components and thus the simultaneous removal efficiency of SO2, NOx and Hg0. *Fuel*, *293*, 120391.

Rahali, S., Ben Aissa, M. A., Khezami, L., Elamin, N., Seydou, M., & Modwi, A. (2021). Adsorption behavior of Congo red onto barium-doped ZnO nanoparticles: correlation between experimental results and DFT calculations. *Langmuir*, *37*(24), 7285-7294.

Rashtbari, Y., Afshin, S., Hamzezadeh, A., Abazari, M., Poureshgh, Y., & Fazlzadeh, M. (2020). Application of powdered activated carbon coated with zinc oxide nanoparticles prepared using a green synthesis in removal of Reactive Blue 19 and Reactive Black-5: adsorption isotherm and kinetic models. *Desalination and Water Treatment*, *179*, 354-367.

Sabzehmeidani, M. M., Mahnaee, S., Ghaedi, M., Heidari, H., & Roy, V. A. (2021). Carbon based materials: A review of adsorbents for inorganic and organic compounds. *Materials Advances*, *2*(2), 598-627.

Sana, S. S., Kumbhakar, D. V., Pasha, A., Pawar, S. C., Grace, A. N., Singh, R. P., ... & Peng, W. (2020). Crotalaria verrucosa leaf extract mediated synthesis of zinc oxide nanoparticles: assessment of antimicrobial and anticancer activity. *Molecules*, *25*(21), 4896.

Saputra, A. H., & Putri, R. A. (2017, May). The determination of optimum condition in water hyacinth drying process by mixed adsorption drying method and modified fly ash as an adsorbent. In *AIP Conference Proceedings* (Vol. 1840, No. 1, p. 100005). AIP Publishing LLC.

Sheeja, J., Sampath, K., & Kesavasamy, R. (2021). Experimental Investigations on Adsorption of Reactive Toxic Dyes Using Hedyotis umbellate Activated Carbon. *Adsorption Science & Technology*, *2021*.

Sheng, S., Liu, B., Hou, X., Wu, B., Yao, F., Ding, X., & Huang, L. (2018). Aerobic biodegradation characteristic of different water-soluble azo dyes. *International journal of environmental research and public health*, *15*(1), 35.

Slama, H. B., Chenari Bouket, A., Pourhassan, Z., Alenezi, F. N., Silini, A., Cherif-Silini, H., ... & Belbahri, L. (2021). Diversity of synthetic dyes from textile industries, discharge impacts and treatment methods. *Applied Sciences*, *11*(14), 6255.

Song, M., Jin, B., Xiao, R., Yang, L., Wu, Y., Zhong, Z., & Huang, Y. (2013). The comparison of two activation techniques to prepare activated carbon from corn cob. *Biomass and Bioenergy*, *48*, 250-256.

Srivastava, S., Sinha, R., & Roy, D. (2004). Toxicological effects of malachite green. *Aquatic toxicology*, *66*(3), 319-329.

Suresh, S. (2014). Treatment of textile dye containing effluents. *Current Environmental Engineering*, *1*(3), 162-184.

Swan, N. B., & Zaini, M. A. A. (2019). Adsorption of malachite green and congo red dyes from water: recent progress and future outlook. *Ecological Chemistry and Engineering*, *26*(1), 119-132.

Temkin, M. J., & Pyzhev, V. (1940). Recent modifications to Langmuir isotherms.

Thomas, K. J., Venkateswararao, A., Balasaravanan, R., Li, C. T., & Ho, K. C. (2019). Triazine-branched mono-and dianchoring organic dyes: Effect of acceptor arms on optical and photovoltaic properties. *Dyes and Pigments*, *165*, 182-192.

Torkian, N., Bahrami, A., Hosseini-Abari, A., Momeni, M. M., Abdolkarimi-Mahabadi, M., Bayat, A., ... & Hojjati-Najafabadi, A. (2022). Synthesis and characterization of Ag-ion-exchanged zeolite/TiO2 nanocomposites for antibacterial applications and photocatalytic degradation of antibiotics. *Environmental Research*, *207*, 112157.

Tovar-Jiménez, X., Favela-Torres, E., Volke-Sepúlveda, T. L., Escalante-Espinosa, E., Díaz-Ramírez, I. J., Córdova-López, J. A., & Téllez-Jurado, A. (2019). Influence of the geographical area and morphological part of the water hyacinth on its chemical composition. *Ingeniería agrícola y biosistemas*, *11*(1), 39-52.

Venkateasan, A., Prabakaran, R., & Sujatha, V. (2017). Phytoextract-mediated synthesis of zinc oxide nanoparticles using aqueous leaves extract of Ipomoea pes-caprae (L). R. br revealing its biological properties and photocatalytic activity. *Nanotechnology for Environmental Engineering*, *2*(1), 1-15.

Vijayageetha, V. A., Rajan, A. P., Arockiaraj, S. P., Annamalai, V., Janakarajan, V. N., Balaji, M. S., & Dheenadhayalan, M. S. (2014). Treatment study of dyeing industry effluents using reverse osmosis technology. *Research Journal of Recent Sciences*, *3*(ISC-2013)), 58-61

Waheeb, A. S., Alshamsi, H. A. H., Al-Hussainawy, M. K., & Saud, H. R. (2020). Myristica fragrans shells as potential low cost bio-adsorbent for the efficient removal of rose Bengal from aqueous solution: Characteristic and kinetic study. *Indonesian Journal of Chemistry*, *20*(5), 1152-1162.

Wong, S., Ghafar, N. A., Ngadi, N., Razmi, F. A., Inuwa, I. M., Mat, R., & Amin, N. A. S. (2020). Effective removal of anionic textile dyes using adsorbent synthesized from coffee waste. *Scientific reports*, *10*(1), 1-13.

Xu, J., Chen, L., Qu, H., Jiao, Y., Xie, J., & Xing, G. (2014). Preparation and characterization of activated carbon from reedy grass leaves by chemical activation with H3PO4. *Applied Surface Science*, *320*, 674-680.

Yan, B., Zheng, J., Wang, F., Zhao, L., Zhang, Q., Xu, W., & He, S. (2021). Review on porous carbon materials engineered by ZnO templates: Design, synthesis and capacitance performance. *Materials & Design*, *201*, 109518.

Yassin, M. T., Mostafa, A. A. F., Al-Askar, A. A., & Al-Otibi, F. O. (2022). Facile Green Synthesis of Zinc Oxide Nanoparticles with Potential Synergistic Activity with Common Antifungal Agents against Multidrug-Resistant Candidal Strains. *Crystals*, *12*(6), 774.

Zafar, M. N., Dar, Q., Nawaz, F., Zafar, M. N., Iqbal, M., & Nazar, M. F. (2019). Effective adsorptive removal of azo dyes over spherical ZnO nanoparticles. *Journal of Materials Research and Technology*, *8*(1), 713-725.

Zaheer, Z., Bawazir, W. A., Al-Bukhari, S. M., & Basaleh, A. S. (2019). Adsorption, equilibrium isotherm, and thermodynamic studies to the removal of acid orange 7. *Materials Chemistry and Physics*, *232*, 109-120.